ORNL/TM-2022/2751

Outdoor Test Bed Performance of a Power Line Sensor Using a Real-Time Event Simulator

Emilio C. Piesciorovsky
R. J. “Bruce” Warmack
Jason K. Richards
Yarom Polsky

November 2022

OAK RIDGE National Laboratory

ORNL IS MANAGED BY UT-BATTELLE LLC FOR THE US DEPARTMENT OF ENERGY

ORNL/TM-2022/2751

Electrification and Energy Infrastructures Division

OUTDOOR TEST BED PERFORMANCE OF A POWER LINE SENSOR USING A REAL-TIME EVENT SIMULATOR

Emilio C. Piesciorovsky
R. J. "Bruce" Warmack
Jason K. Richards
Yarom Polsky

November 2022

Prepared by
OAK RIDGE NATIONAL LABORATORY
Oak Ridge, TN 37831-6283
managed by
UT-BATTELLE LLC
for the
US DEPARTMENT OF ENERGY

CONTENTS

LIST OF FIGURES

LIST OF TABLES

ABBREVIATIONS

COMTRADE	common format for transient data exchange
CT	current transformer
DECC	Distributed Energy Communications and Control
EPB	Electric Power Board of Chattanooga
G&W	Gear & Williams Electric
LL	line to line
LLG	line to line ground
OPLS	outdoor power line sensor
OPLST	outdoor power line sensor test bed
ORNL	Oak Ridge National Laboratory
PT	potential transformer
SEL	Schweitzer Engineering Laboratories
3LG	three-line to ground

EXECUTIVE SUMMARY

This report summarizes the design and application of an outdoor power line sensor test bed (OPLST) with a real-time simulator and power meter to compare a potential transformer (PT) and current transformer (CT) vs. an advanced outdoor power line sensor (OPLS). The OPLST was created to validate advanced medium-voltage (20/34.5 kV) OPLSs used in electrical distribution systems. Electrical utilities have installed metering and relay protection transformers such as PTs and CTs for several decades. The PTs/CTs are iron core measurement transformers based on the electromagnetic induction principle and provide reliable data in normal grid operation. However, new OPLSs using other technologies such as voltage dividers, Rogowski coils, and optical principles have become available and may have favorable performance and costs compared with PTs/CTs. Therefore, the importance of testing these technologies with the PT/CT to compare the measured phase voltage/current at different power grid scenarios is crucial to understand the performance of these new OPLSs.

For this study, a G&W Model CVS-36-O power line sensor was chosen as the OPLS to test with voltage/current signals. An OPAL-RT Technologies Model OP4510 real-time simulator and SEL-735 power meter were installed with the 20/34.5 kV OPLST to compare the measured transient events collected from an advanced OPLS and the PT/CT. This system is installed at the Distributed Energy Communications and Control lab at the US Department of Energy's Oak Ridge National Laboratory. The simulator generated different power grid scenarios (e.g., electrical faults, capacitor bank operation, service restoration), and its analog-output signals were connected to the voltage/current amplifiers that feed the 20/34.5 kV aerial cable loop through the PT/CT devices. Additional PT/CT devices were also wired with the medium-voltage aerial cable loop to measure the phase current/voltage signals and server as references. After each test, common format for transient data exchange files were collected from the SEL-735 power meter and used to compare the performance of the OPLS with the PT/CT. The behavior of analog signals, harmonic components, total harmonic distortion, and crest factors were assessed and found favorable for the G&W sensor as compared with the reference PT/CT.

1. INTRODUCTION

In electrical substations, the metering from protective relays (or power meters) is performed through potential transformers (PTs) and current transformers (CTs) for measuring phase voltages and currents, and these devices are commissioned by electrical engineers [1]. The PTs/CTs can detect and react to various electrical anomalies that could adversely affect the electrical grid operations. However, most protective relays have low sampling frequencies and cannot detect high harmonic events that are related to incipient power outages [2]. The computational process for protective relays and power meters for measuring transient events with high-frequency components at electrical faults must process the phase voltage and current signals with small time steps. This computational process depends on the sampling frequency related to the Nyquist sampling theorem [3] so that the sampling frequency of a signal should be at least twice the highest frequency of the signal to avoid aliasing [3]. Another aspect of measurement transformers built by magnetic iron cores is that the performance of CTs could be affected by the magnetic saturation errors with high-current faults in the power grid [4, 5], yielding ratio and phase angle errors [6], especially during transient power grid events.

Additionally, the global use of solar and wind power has grown rapidly, with accelerating growth in recent years [7] such that the use of inverter-based distributed energy resources has increased along with electronic solid-state switches to control microgrid systems [8]. These devices could provide high-harmonic components into the microgrids that could affect the power quality and grid reliability [9]. Consequently, the need of using more accurate high-speed sensors to measure and control the electrical power grids is crucial for detecting these events.

In electrical utility substations and labs, PT and CT test equipment have been used by electrical engineers to assess traditional measurement transformers for several decades [10, 11]. Today, PT and CT test equipment are based on a microprocessor-based single–phase or three–phase turn ratio testers that allow for assessing the PTs/CTs [12, 13]. The PT and CT test equipment are analyzers that inject the analog signals into the PT/CT and determine their equivalent circuit parameters and performance. The CT test equipment can perform different tests such as the voltage excitation, ratio, polarity, phase angle, and winding resistance and insulation measurement [14]. The PT test equipment can perform several tests such as the current excitation, ratio, polarity, power factor, and winding resistance and insulation measurements [15]. Generally, research test beds used for power line sensors are set on indoor sites instead of outdoor. In such cases, sensors are only tested at a room environment instead of real-weather conditions and gauge the magnitude and phase of voltage/current signals under limited conditions [16]. Furthermore, these research test beds do not compare the performance of outdoor power line sensors (OPLSs) with that of a PT/CT.

Modern voltage and current sensing solutions include optical sensors, air-core coil-based sensors, resistive and capacitive dividers, and hybrid solutions that have gained increasing interest for use in the digital electrical power grid [17]. In addition, some electrical utilities have started to install these new sensor technologies for experimental monitoring applications. For instance, in collaboration with the US Department of Energy's Oak Ridge National Laboratory (ORNL), the Electric Power Board of Chattanooga (EPB) installed optical power line sensors (26.6 kV phase to neutral voltage) to measure the phase currents and voltages at this 46 kV EPB electrical substation [18]. Advanced sensor technologies have been focused on simplifying the installation, improving the reliability of power delivery, enhancing the detection of electrical faults, and observing transient events. However, it is unknown if these advanced power line sensors could replace or supplement traditional PTs/CTs in electric distribution systems for anomaly detection and/or transient events high frequency components. Therefore, comparing traditional PTs/CTs against the advanced voltage/current sensors will be crucial in assessing the performance of these new technologies. Comparing traditional and advanced technologies is the goal of the present study

using the novel OPLS test bed (OPLST) over a full range of operating conditions for new power line sensors alongside iron-core PTs/CTs up to 20/34.5 kV.

In this study, the OPLST with an OP4510 real-time simulator and SEL-735 power meter was constructed at the Distributed Energy Communications and Control (DECC) lab at ORNL. This novel medium-voltage OPLST consists of an aluminum aerial cable that represents a medium-voltage aerial cable loop. The outdoor PTs/CTs together with advanced power line sensors were connected along this aerial cable loop. The OPLST with a real-time simulator and power meter enable testing of conventional PT/CT and advanced power line sensors at different electrical grid operation conditions, such as electrical faults, capacitor banks connection, and energy restoring services. Table 1 describes the novelties of the OPLST vs. the PT/CT test equipment, indicating types of tests and metering.

Table 1. Novelties of the medium-voltage OPLST vs. the PT/CT test equipment

Methods	Types	CTs	PTs	Outdoor advanced power line sensors
Manufacturer test equipment	Tests	• Voltage excitation test • Ratio and polarity test	• Current excitation test • Ratio and polarity test	—
	Metering	• Measurement of phase angle • Measurement of winding resistant and insulation	• Measurement of power factor • Measurement of winding resistant and insulation	—
20/34.5 kV OPLST with real-time simulator and power meter	Tests	• Comparison of the OPLS vs. the PT/CT • Outdoor testing		
	Metering	• Measurement of power grid test scenarios such as electrical faults (SLG, LLG, LL, 3LG) and load feeder and capacitor bank breaker operations • Measurement of voltage and current signals with up to 512 samples/cycle • Measurement of total harmonic distortion for voltage and current signals • Measurement of crest factor for voltage and current signals		

SLG: single-line to ground, LLG: line to line ground, LL: line to line, 3LG: three-line to ground

In the medium-voltage OPLST, the analog signals from the outdoor 20/34.5 kV PT (ratio = 175:1, accuracy = 0.15Y) and CT (ratio = 400:5 A, accuracy = 0.15SB-1.8) vs. the OPLS (G&W Model CVS-36-O) were measured and compared. The OPLST with the real-time simulator and high-sampling frequency power meter has the advantage that electrical grid transient event tests can be simulated and performed as often as desired, instead of at an electrical substation site where events only rarely occur. Since the OPLST is single-phase, sequential playback of events is performed for phase A, B, and C. In the OPLST, the analog signals from the real-time simulator were amplified in two steps, first by the voltage/current amplifiers, and then by a PT/CT that injected the voltage and current signals to the aerial cable loop. In addition, the SEL-735 power meter with the low-level signal interface was used to measure the phase current/voltage signals of real-time simulator, PT/CT, and OPLS with all current/voltage signals recorded at the same test event by the power meter.

2. THEORY AND EQUATIONS

In this section, the definitions and equations for the individual harmonic component, total harmonic distortion, and crest factor of the voltage and current signals are defined. In addition, the definitions and equations of the percentage errors for the total harmonic distortion and crest factor at voltage/current signals are presented. These equations were used to provide the analysis and comparison of the OPLS vs. the PT/CT.

2.1 INDIVIDUAL HARMONIC COMPONENT

The individual harmonic component for voltage and current signals are usually plotted in frequency plots for harmonic analysis. The individual harmonic component for the voltage and current signals are defined as the percentage of harmonics at the *n* generic harmonic component with respect to the fundamental signal of 60 Hz. The individual harmonic components of the voltage and current signals are calculated by Eqs. (1) and (2), respectively.

$$V_{n\%} = \frac{V_n}{V_1} \times 100 \, , \tag{1}$$

where $V_{n\%}$ is individual harmonic component of the *n* generic harmonic for the phase voltage signal as a percentage, V_n is the phase voltage magnitude of the *n* generic harmonic component signal in volts, and V_1 is the phase voltage magnitude of the fundamental signal in volts.

$$I_{n\%} = \frac{I_n}{I_1} \times 100 \, , \tag{2}$$

where I_n is individual harmonic component of the *n* generic harmonic for the phase current signal as a percentage, I_n is the phase current magnitude of the *n* generic harmonic component signal in amps, and I_1 is the phase current magnitude of the fundamental signal in amps.

2.2 TOTAL HARMONIC DISTORTION FACTOR

The total harmonic distortion for the phase voltage and current signals at different power grid scenarios were compared for the OPLS vs. the PT/CT. In power grid systems, voltages and currents have harmonics with frequencies that are integer multiples of the waveform's fundamental frequency. For example, given a 60 Hz fundamental waveform, the 2nd, 3rd, 4th, and 5th harmonic components will be at 120, 180, 240, and 300 Hz, respectively. The total harmonic distortion is the degree to which a waveform deviates from a pure sinusoid at its fundamental frequency (e.g., 60 Hz). The ideal sine wave has no higher harmonic components. In that case, there is nothing to distort this perfect wave. The total harmonic distortion is the summation of all harmonic components of the voltage or current waveform compared with the fundamental component of the voltage or current wave. The total harmonic distortion for the phase voltage and current signals can be estimated by Eqs. (3) and (4), respectively.

$$THD_V = \frac{\sqrt{\sum_{n=2}^{10} V_n^2}}{V_1} \times 100 \, , \tag{3}$$

where THD_V is total harmonic distortion for the phase voltage signal as a percentage, V_n is the phase voltage magnitude of the *n* generic harmonic component signal in volts, and V_1 is the phase voltage magnitude of the fundamental signal in volts.

$$THD_I = \frac{\sqrt{\sum_{n=2}^{10} I_n^2}}{I_1} \times 100 \, , \tag{4}$$

where THD_I is total harmonic distortion for the phase current signal as a percentage, I_n is the phase current magnitude of the n generic harmonic component signal in amps, and I_1 is the phase current magnitude of the fundamental signal in amps.

2.3 CREST FACTOR

The crest factor for the voltage and current signals at different power grid scenarios were compared for the OPLS vs. the PT/CT. The crest factor is defined as the ratio between the peak value and its root mean square value. The crest factor of a perfect sinusoidal is 1.414. The crest factor for the voltage and current signals can be estimated by Eqs. (5) and (6), respectively.

$$CF_V = \frac{V_{peak}}{V_{rms}}, \tag{5}$$

where CF_V is the crest factor for the voltage signal, V_{peak} is the peak value in volts, and V_{rms} is the root mean square value in volts.

$$CF_I = \frac{I_{peak}}{I_{rms}}, \tag{6}$$

where CF_I is the crest factor for the phase current signal, I_{peak} is the phase current peak value in amps, and I_{rms} is the phase current root mean square value in amps.

2.4 PERCENTAGE ERRORS OF TOTAL HARMONIC DISTORTION AND CREST FACTOR

The percentage errors for the total harmonic distortion and crest factor of the measured phase voltage/current signals between the PT/CT and the OPLS were calculated. The percentage error for the total harmonic distortion of the measured phase voltage and current can be estimated by Eqs. (7) and (8), respectively.

$$E_{\%\,THDV} = \frac{THD_{VOPLS} - THD_{VPT}}{THD_{VPT}}, \tag{7}$$

where $E_{\%\,THDV}$ is the percentage error of the phase voltage total harmonic distortion as a percentage, THD_{VOPLS} is the phase voltage total harmonic distortion of the OPLS as a percentage, and THD_{VPT} is the phase voltage total harmonic distortion of the PT as a percentage.

$$E_{\%\,THDI} = \frac{THD_{IOPLS} - THD_{ICT}}{THD_{ICT}}, \tag{8}$$

where $E_{\%\,THDI}$ is the percentage error of the phase current total harmonic distortion as a percentage, THD_{IOPLS} is the phase current total harmonic distortion of the OPLS as a percentage, and THD_{ICT} is the phase current total harmonic distortion of the CT as a percentage.

Consequently, the percentage error for the crest factor of the measured phase voltage and current signals can be estimated by Eqs. (9) and (10), respectively.

$$E_{\%\,CFV} = \frac{CF_{VOPLS} - CF_{VPT}}{CF_{VPT}} \times 100, \tag{9}$$

where $E_{\%\,CFV}$ is the percentage error of the phase voltage crest factor as a percentage, CF_{VOPLS} is the phase voltage crest factor of the OPLS, and CF_{VPT} is the phase voltage crest factor of the PT.

$$E_{\%\,CFI} = \frac{CF_{IOPLS} - CF_{ICT}}{CF_{ICT}} \times 100\ , \tag{10}$$

where $E_{\%\,CFI}$ is the percentage error of the phase current crest factor as a percentage, CF_{IOPLS} is the phase current crest factor of the OPLS, and CF_{ICT} is the phase current crest factor for the CT.

3. THE OPLST

In this section, the diagram of the OPLST is presented. Next, the process of calculating the voltage/current gains at the OPLST by using the high-voltage/-current and low-voltage interfaces of analog signals at the power meter is described in detail. The equipment and rack unit for the OPLST set in the DECC lab are defined. Finally, the software, settings, and operational steps of the OPLST are presented.

3.1 DIAGRAM OF THE MEDIUM-VOLTAGE OPLST

The diagram of the medium-voltage OPLST is shown in Figure 1. The outside dashed line (Figure 1A) shows the 20/34.5 kV aerial cable loop with the PT/CT and the OPLS (G&W Model CVS-36-O), and the inside the dashed line (Figure 1B) shows equipment installed in the rack unit (indoor). The rack unit (Figure 1B) has an OP4510 real-time simulator, an SEL-735 power meter, and current/voltage amplifiers.

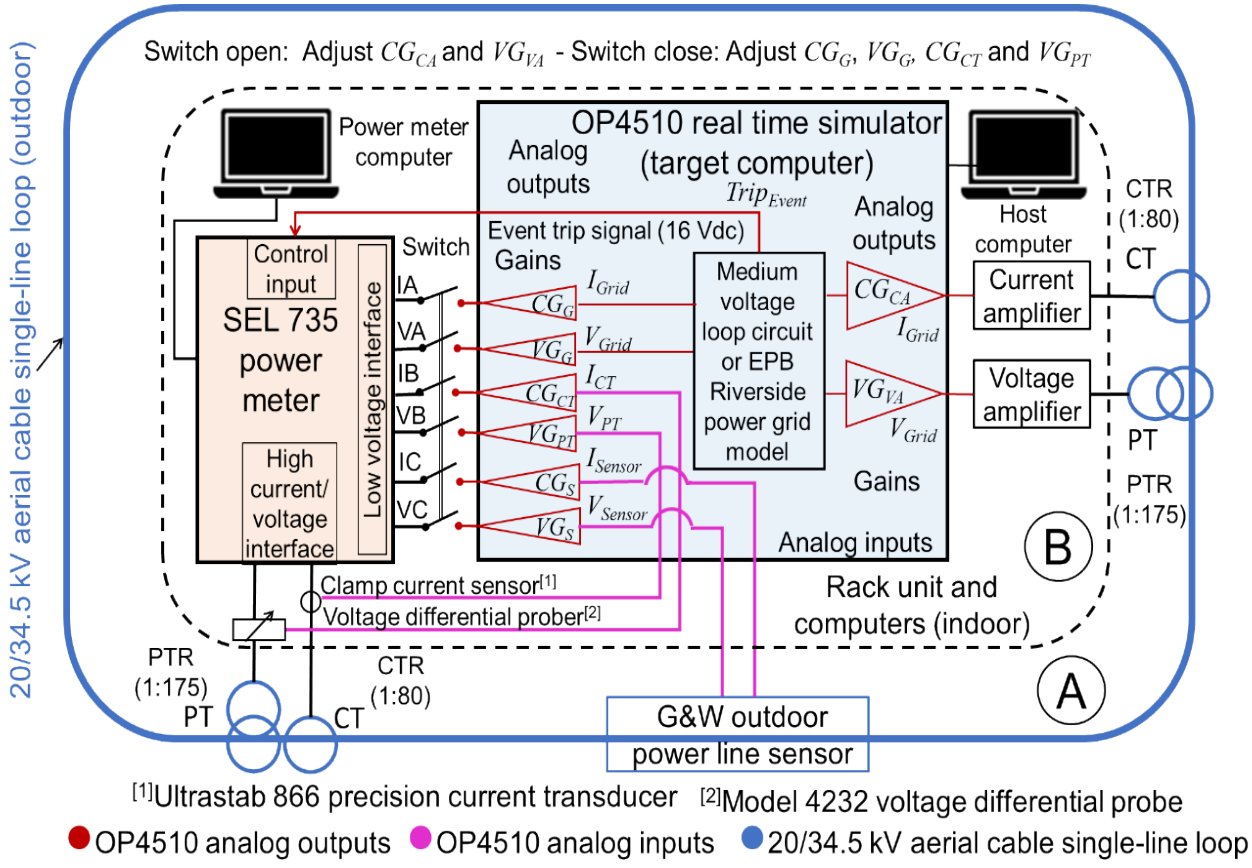

Figure 1. Diagram of test bed with 20/34.5 kV aerial cable loop (A) and rack unit (B).

The OP4510 real-time simulator was connected to a host computer to run the tests, and the SEL-735 power meter was connected to another computer to collect the events after running the tests. The OP4510 real-time simulator has analog inputs and outputs. The analog inputs were connected to the PT/CT and to the G&W power line sensor, and the analog outputs were connected to the power meter and voltage/current amplifiers (Figure 1B).

The SEL-735 power meter was connected to the high-voltage/-current interface and the low-voltage interface. In Figure 1B, by opening the switch of the low-voltage interface, the high-voltage/-current interface was enabled, and it was used to adjust the gains of the amplifiers (CG_{CA}, VG_{VA}) for the real-time simulator. However, by closing the switch of the low-voltage interface, the high-current/-voltage interface was disabled, and the low-voltage interface was used to adjust the gains of the simulated medium-voltage loop circuit or power grid (CG_G, VG_G) and PT/CT (VG_{PT}, CG_{CT}) for the real-time simulator.

In Figure 1B, the voltage (VG_{VA}, VG_G, VG_{PT}, VG_S) and current (CG_{CA}, CG_G, CG_{CT}, CG_S) gains for analog outputs were calculated to set the RT-LAB project in the OP4510 real-time simulator. Essentially, the gains to connect the SEL-735 power meter were calculated using the voltage (750 V/V) and current (16.53 A/V) scaling factors of the low-voltage interface. However, the gains to connect the voltage/current amplifiers were calculated using the amplifier gains and PT/CT ratios that were wired between the amplifiers and the medium-voltage aerial cable loop.

From the low-voltage interface (Figure 1B), phase A measures the voltage/current of the simulated medium-voltage loop circuit or power grid, phase B measures the voltage/current of the PT/CT, and phase C measures the voltage/current of the G&W OPLS. To record the phase A, B, and C voltage/current signals during the tests, the OP4510 real-time simulator generated a 16 Vdc trip signal (Figure 1B) that enabled tripping the recording of the test events inside the SEL-735 power meter.

3.2 VOLTAGE AND CURRENT GAINS FOR THE OP4510 REAL-TIME SIMULATOR

In the medium-voltage OPLST, the OP4510 real-time simulator (Figure 1B) was the main interconnection to adapt the voltage and current signals from all devices. The voltage and current gains were calculated for the low-voltage interface of the SEL-735 power meter, and the voltage/current amplifiers. Table 2 lists the voltage and current gains of the OP4510 real-time simulator. The gains of the amplifiers, power grid, and PT/CT for the OP4510 real-time simulator were calculated. The voltage and current gains were calculated and then adjusted using the OP4510 real-time simulator and SEL-735 power meter.

In the voltage and current gains of the amplifiers (Figure 1B) for the OP4510 real-time simulator, the OP4510 real-time simulator simulated the medium-voltage loop circuit or power grid that generated the voltage and current signals. Then, these signals were scaled with the gains for the voltage (GV_{VA}) and current (GC_{CA}) amplifiers. The voltage and current amplifiers feed the PT and CT, respectively, to inject the desired voltage and current at the medium-voltage aerial cable loop (Figure 1A).

In the voltage and current gains of the SEL-735 power meter (Figure 1B) for the OP4510 real-time simulator, the voltage and current signals for the simulated medium-voltage loop circuit or power grid were connected to the voltage (VG_G) and current (CG_G) gains. The PT and CT signals were measured by a differential-voltage probe and current sensor, respectively. Then, these sensor signals were scaled with the PT voltage (VG_{PT}) and CT current (CG_{CT}) gains connected to the low-voltage interface of the SEL-735 power meter. In addition, the voltage and current signals from the G&W power line sensor were scaled with the sensor voltage (VG_S) and current (CG_S) gains. Then, voltage/current signals from the G&W power line sensor vs. the PT/CT were referenced at the same SEL-735 power meter to compare the voltage/current signals from the G&W power line sensor vs. the PT/CT.

Table 2. Voltage and current gains for the OP4510 real-time simulator

Gain (ID)	Gain interface	Gain area	Gain function	Gain value calculated (adjusted)	Equation
Voltage gain of the voltage amplifier (VG_{VA})	20/34.5 kV aerial cable loop	Grid simulation	To scale the voltage signal from the simulated power grid to the voltage amplifier and PT	0.00028571 (0.00028492)	Eq. (11)
Current gain of the current amplifier (CG_{CA})			To scale the current signal from the simulated power grid to the current amplifier and CT	0.11363636 (0.11172054)	Eq. (12)
Voltage gain of the simulated grid (VG_G)	Low-voltage interface of SEL-735 power meter	Grid simulation	To scale the voltage signal from the simulated power grid to the SEL-735 power meter[a]	1/131,250 (1/130,903)	Eq. (13)
Current gain of the simulated grid (CG_G)			To scale the current signal from the simulated power grid to the SEL-735 power meter[a]	1/1,322.4 (1/1,315.5)	Eq. (14)
Voltage gain of the PT (VG_{PT})		PT/CT	To scale the voltage signal from the PT to the SEL-735 power meter[a]	0.13333333 (0.13383402)	Eq. (15)
Current gain of the CT (CG_{CT})			To scale the current signal from the CT to the SEL-735 power meter[a]	0.30248033 (0.30130787)	Eq. (18)
Voltage gain of the G&W sensor (VG_S)		G&W sensor	To scale the voltage signal from the G&W sensor to the SEL-735 power meter[a]	0.038095	Eq. (19)
Current gain of the G&W sensor (CG_S)			To scale the current signal from the G&W sensor to the SEL-735 power meter[a]	2.520	Eq. (20)

[a]Connected to the low voltage level interface of the SEL-735 power meter

3.3 CALCULATION OF VOLTAGE AND CURRENT GAINS FOR AMPLIFIERS AT THE OP4510 REAL-TIME SIMULATOR

The voltage and current amplifiers used in the OPLST are the AE TECHRON Model 7228 [19]. These linear amplifiers can be used as single units or connected in series or parallel to increase the voltage or current outputs, respectively. However, these were used as single units by connecting one as a voltage-to-current amplifier and another as a voltage amplifier. The manufacturer default voltage and current gains of these amplifiers is 20 V/V and 5 A/V, respectively [19]. However, these gains were set by the gain control knob that can increase/decrease the gain between 0% and 100% [19]. The voltage and current gains were approximately set at 20 V/V and 0.11 A/V, respectively. The voltage (VG_{VA}) and current (CG_{CA}) gains of the amplifiers for the OP4510 real-time simulator were calculated by using Eqs. (11) and (12), respectively.

$$VG_{VA} = \frac{1}{G_{VA} \times PTR_L} = \frac{1}{20\frac{V}{V} \times 175} = 0.00028571\ , \tag{11}$$

where VG_{VA} is the voltage gain of the voltage amplifier for the OP4510 real-time simulator, G_{VA} is the selected gain of the voltage amplifier in V/V, and PTR_L is the ratio of the PT connected between the voltage amplifier and the medium-voltage aerial cable loop.

$$CG_{CA} = \frac{1}{G_{CA} \times CTR_L} = \frac{1}{0.11 \frac{A}{V} \times 80} = 0.11363636\ , \tag{12}$$

where CG_{CA} is the current gain of the current amplifier for the OP4510 real-time simulator, G_{CA} is the selected gain of the current amplifier in A/V, and CTR_L is the ratio of the CT connected between the current amplifier and the medium-voltage aerial cable loop.

3.4 CALCULATION OF VOLTAGE AND CURRENT GAINS FOR THE SEL-735 POWER METER AT THE OP4510 REAL-TIME SIMULATOR

In the OPLST (Figure 1), the SEL-735 power meter measured the voltage and current signals, and the OP4510 real-time simulator was the main interface between the SEL-735 power meter and the test bed devices. Therefore, the voltage/current gains of the simulated medium-voltage loop circuit or power grid, PT/CT, and G&W power line sensor were calculated for the OP4510 real-time simulator based on Table 2.

The voltage and current gains of the simulated medium-voltage loop circuit or power grid for the OP4510 real-time simulator were calculated by Eqs. (13) and (14), respectively.

$$VG_G = \frac{1}{VSF_M \times PTR_M} = \frac{1}{750 \frac{V}{V} \times 175} = \frac{1}{131{,}250}\ , \tag{13}$$

where VG_G is the voltage gain of the simulated medium-voltage loop circuit or power grid for the OP4510 real-time simulator, VSF_M is the voltage scaling factor of the SEL-735 power meter in V/V, and PTR_M is the PT ratio set in the SEL-735 power meter.

$$CG_G = \frac{1}{CSF_M \times CTR_M} = \frac{1}{16.53 \frac{A}{V} \times 80} = \frac{1}{1{,}322.4}\ , \tag{14}$$

where CG_G is the current gain of the simulated medium-voltage loop circuit or power grid for the OP4510 real-time simulator, CSF_M is the current scaling factor of the SEL-735 power meter in A/V, and CTR_M is the CT ratio set in the SEL-735 power meter.

The voltage and current gains of the PT/CT for the OP4510 real-time simulator were calculated to connect the PT/CT signals at the low-voltage interface of the SEL-735 power meter. Therefore, a differential voltage probe and clamp current sensor were used to collect the PT/CT signals with the OP4510 real-time simulator (Figure 1B).

For the PT connected to the SEL-735 power meter (Figure 1B), the voltage signal was collected by a Model 4232 differential voltage probe [20] that has a voltage scaling factor of 100 V/V. The voltage gain of the PT for the OP4510 real-time simulator is given by Eq. (15).

$$VG_{PT} = \frac{VSF_{DP}}{VSF_M} = \frac{100 \frac{V}{V}}{750 \frac{V}{V}} = 0.13333333\ , \tag{15}$$

where VG_{PT} is the voltage gain of the PT for the OP4510 real-time simulator, VSF_{DP} is the voltage scaling factor of the Model 4232 voltage differential probe in V/V, and VSF_M is the voltage scaling factor of the SEL-735 power meter in V/V.

For the CT connected to the SEL-735 power meter (Figure 1B), the current signal was collected by an Ultrastab 866 precision current transducer [21] with a current transfer ratio of 1,500:1, three turns of

primary cable, and a burden external resistor impedance of 100 ohms. Figure 2 shows the circuit of the Ultrastab 866 precision current transducer.

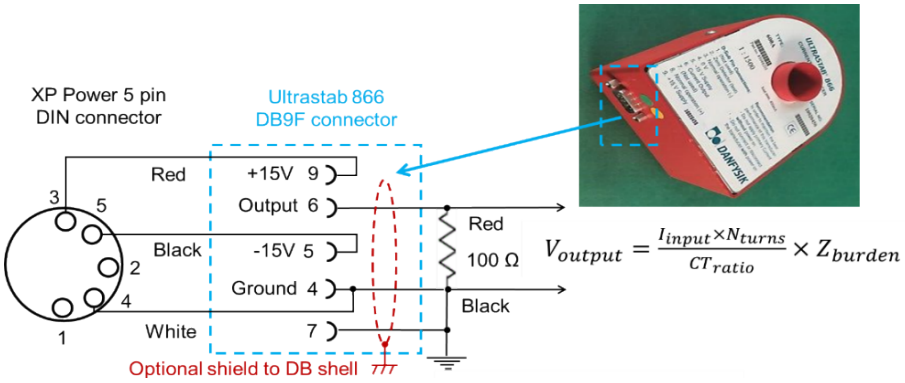

Figure 2. Circuit of the Ultrastab 866 precision current transducer.

From Figure 2 and Eqs. (16) and (17) , the current scaling factor for the Ultrastab 866 precision current transducer (CSF_{U866}) was 5 A/V.

$$V_{output} = \frac{I_{input} \times N_{turns}}{CT_{ratio}} \times Z_{burden} \,, \tag{16}$$

$$CSF_{U866} = \frac{I_{input}}{V_{output}} = \frac{CT_{ratio}}{N_{turns} \times Z_{burden}} = \frac{1500}{3 \times 100} = 5\,\frac{A}{V} \,, \tag{17}$$

where V_{output} is the output voltage in volts, I_{input} is the input current in amps, N_{turns} is the number of turns of primary cable, CT_{ratio} is the current transfer ratio of the Ultrastab 866 precision current transducer (1,500:1), and Z_{burden} is the burden external resistor impedance in ohms.

Since the CT was connected to the Ultrastab 866 precision current transducer, the current gain of the CT for the OP4510 real-time simulator was calculated by Eq. (18).

$$CG_{CT} = \frac{CSF_{U866}}{CSF_M} = \frac{5\,\frac{A}{V}}{16.53\,\frac{A}{V}} = 0.30248033 \,, \tag{18}$$

where CG_{CT} is the current gain of the CT for the OP4510 real-time simulator, CSF_{U866} is the current scaling factor of the Ultrastab 866 precision current transducer in A/V, and CSF_M is the current scaling factor of the SEL-735 power meter in A/V.

The voltage and current gains of the G&W power line sensor for the OP4510 real-time simulator were calculated by Eqs. (19) and (20), respectively. The voltage (5,000 V/V) and current (3,333.3 A/V)/scaling factors of the G&W power line sensor; voltage (750 V/V) and current (16.53 A/V) scaling factors of the SEL-735 power meter; and the PT ratio (175:1) and CT ratio (80:1) set in the SEL-735 power meter were needed in this calculation.

$$VG_S = \frac{VSF_S}{VSF_M \times PTR_M} = \frac{5{,}000\,\frac{V}{V}}{750\,\frac{V}{V} \times 175} = 0.038095 \,, \tag{19}$$

where VG_S is the voltage gain of the G&W power line sensor for the OP4510 real-time simulator, VSF_S is the voltage scaling factor of the G&W sensor in V/V, VSF_M is the voltage scaling factor of the SEL-735 power meter in V/V, and PTR_M is the PT ratio set in the SEL-735 power meter.

$$CG_S = \frac{CSF_{G\&W}}{CSF_M \times CTR_M} = \frac{3{,}333.3\,\frac{A}{V}}{16.53\,\frac{A}{V} \times\ 80} = 2.520\ , \tag{20}$$

where CG_S is the current gain of the G&W power line sensor for the OP4510 real-time simulator, CSF_S is the current scaling factor of the G&W sensor in A/V, CSF_M is the current scaling factor of the SEL-735 power meter in A/V, and CTR_M is the CT ratio set in the SEL-735 power meter.

3.5 ADJUSTMENT OF VOLTAGE AND CURRENT GAINS

The calculated voltage and current gains for the OP4510 real-time simulator were adjusted by creating an RT-LAB project that simulated a medium-voltage loop circuit. This circuit was formed by a sinusoidal source and an impedance in series (Figure 3A) that simulated a line to ground voltage of 19.9 kV and a phase current of 80 A. The adjusting process of the gains for the OP4510 real-time simulator was based on running the simulation test of the medium-voltage loop circuit and comparing the measurements from the display of the SEL-735 power meter (Figure 3B). The calculated gains with Eqs. (11), (12), (13), (14), (15), and (18) were initially set in the model (Figure 3C). Then, these values were adjusted up to match the conditions described in Table 3.

Table 3. Adjustment of voltage and current gains for the OP4510 real-time simulator

Gains (ID)	SEL-735 power meter		Conditions
	Connect interface	Measure phase (device)	
Voltage gain of voltage amplifier (VG_{VA})	H	VB* (PT)	Adjusted up to match the PT/CT measurements (phase B voltage/current from the SEL-735 power meter with the high-voltage/-current interface) vs. the voltage/current simulated at the medium-voltage loop circuit (Figure 3A)
		V simulated	
Current gain of current amplifier (CG_{CA})	H	IB* (CT)	
		I simulated	
Voltage gain of simulated grid (VG_G)	H	VB* (PT)	Adjusted up to match the PT/CT measurements (phase B voltage/current from the SEL-735 power meter with the high-voltage/-current interface) vs. the simulated medium-voltage loop circuit measurements (phase A voltage/current from the SEL-735 power meter with the low-voltage interface)
	L	VA (grid)	
Current gain of simulated grid (CG_G)	H	IB* (CT)	
	L	IA (grid)	
Voltage gain of PT (VG_{PT})	H	VB* (PT)	Adjusted up to match the PT/CT signal (phase B voltage/current from the SEL-735 power meter with the low-voltage interface) vs. the PT/CT signal (phase B voltage/current from the SEL-735 power meter with the high-voltage/-current interface)
	L	VB (PT)	
Current gain of CT (CG_{CT})	H	IB* (CT)	
	L	IB (CT)	

H: high-current/-voltage interface, L: low-voltage interface, VA: measured phase A voltage from the SEL-735 power meter, VB: measured phase B voltage from the SEL-735 power meter, VC: measured phase C voltage from the SEL-735 power meter, IA: measured phase A current from the SEL-735 power meter , IB: measured phase B current from the SEL-735 power meter, IC: measured phase C current from the SEL-735 power meter, *Measurement use as main reference in the adjustment of voltage/current gains

The gains of the amplifiers (VG_{VA}, CG_{CA}) for the OP4510 real-time simulator were adjusted by using as a reference the measured voltage/current from the PT/CT of phase B at the high-voltage/-current interface in the SEL-735 power meter, which represented the real voltage/current from the outdoor medium-voltage aerial cable loop in the OPLST. These gains were adjusted by Eq. (21).

$$G'_{ADJ} = G'_{CALC} \times \frac{M_H}{S_{GRID}}\ , \tag{21}$$

where G'_{ADJ} are the adjusted voltage/current gains of amplifiers for the OP4510 real-time simulator, G'_{CALC} are the calculated voltage/current gains of amplifiers from Eqs. (11) and (12), M_H are the measured phase B voltage/current values that were collected by using the high-voltage/-current interface, and S_{GRID} are the simulated phase voltage/current values measured from the voltage and current displays of the 20/34.5 kV loop circuit (Figure 3A).

Also, the gains of the simulated grid (VG_G, CG_G) and PT/CT (VG_{PT}, CG_{CT}) for the OP4510 real-time simulator were adjusted by using as reference the measured the voltage/current from the PT/CT of phase B at the high-voltage/-current interface in the SEL-735 power meter. These gains were adjusted by Eq. (22).

$$G_{ADJ} = G_{CALC} \times \frac{M_H}{M_L}, \tag{22}$$

where G_{ADJ} are the adjusted voltage/current gains of the simulated grid and PT/CT for the OP4510 real-time simulator, G_{CALC} are the calculated voltage/current gains from Eqs. (13), (14), (15), and (18), M_H are the measured phase B voltage/current that were collected by using the high-voltage/-current interface, and M_L are the measured phase A or B voltage/current that were collected by using the low-voltage interface based on the conditions in Table 3.

In this adjustment gain process for the OP4510 real-time simulator, when the low-voltage interface was connected at the SEL-735 power meter, the measurements from the high-voltage/-current interface were not available in the SEL-735 power meter's display. During the simulation of the 20/34.5 kV loop circuit tests (Figure 3A) , the low-voltage interface of the SEL-735 power meter was connected and disconnected up to adjusting the voltage/current gains with Eqs. (21) and (22) and based on the conditions shown in Table 3.

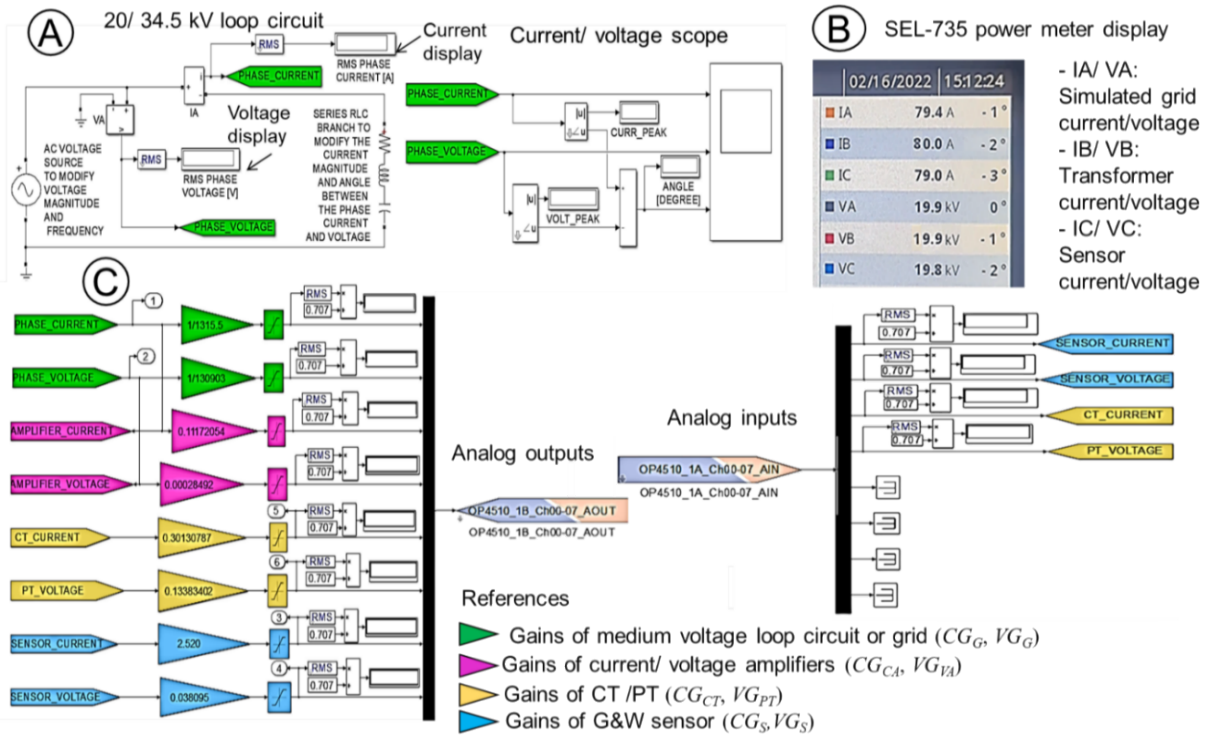

Figure 3. Medium-voltage loop circuit (A), SEL-735 power meter display (B), and current/voltage gains (C).

3.6 MEDIUM-VOLTAGE OPLST

The 20/34.5 kV OPLST (Figure 4A and B) is located outside the DECC lab at ORNL. The OPLST with the OP4510 real-time simulator and SEL-735 power meter was created to perform phase current/voltage transient events at new OPLSs that could be installed in electrical distribution power grids. In the OPLST, the behavior of voltage/current signals from the G&W power line sensor vs. the PT/CT was measured to compare the new voltage/current power line sensor with the traditional iron core measurement transformers. In the medium-voltage OPLST, the G&W power line sensor was a 36 kV-class model CVS-36-O. The PTs were ABB VOG-20B voltage transformers, with a ratio of 20,125:115 V, or a PT ratio of 175, and the CTs were ABB KOR-20ER CTs, with a ratio of 400:5 A, or a CT ratio of 80. In the line pole was set a three-position regular duty bracket (Figure 4B) that enabled mounting of the G&W power line sensor and PT/CT. Inside the DECC lab, the rack unit (Figure 4C) has input/output connectors that enable measuring the analog signals from the medium-voltage OPLST and PT/CT. The SEL-735 power meter was installed on a rack unit, and it recorded the voltage/current signals from the simulated medium-voltage loop circuit or power grid, G&W power line sensor, and PT/CT. Figure 4 shows the medium-voltage aerial cable loop, power line poles, sensors (including others not mentioned in this report), control rack unit, and computers of the medium-voltage OPLST in the DECC lab.

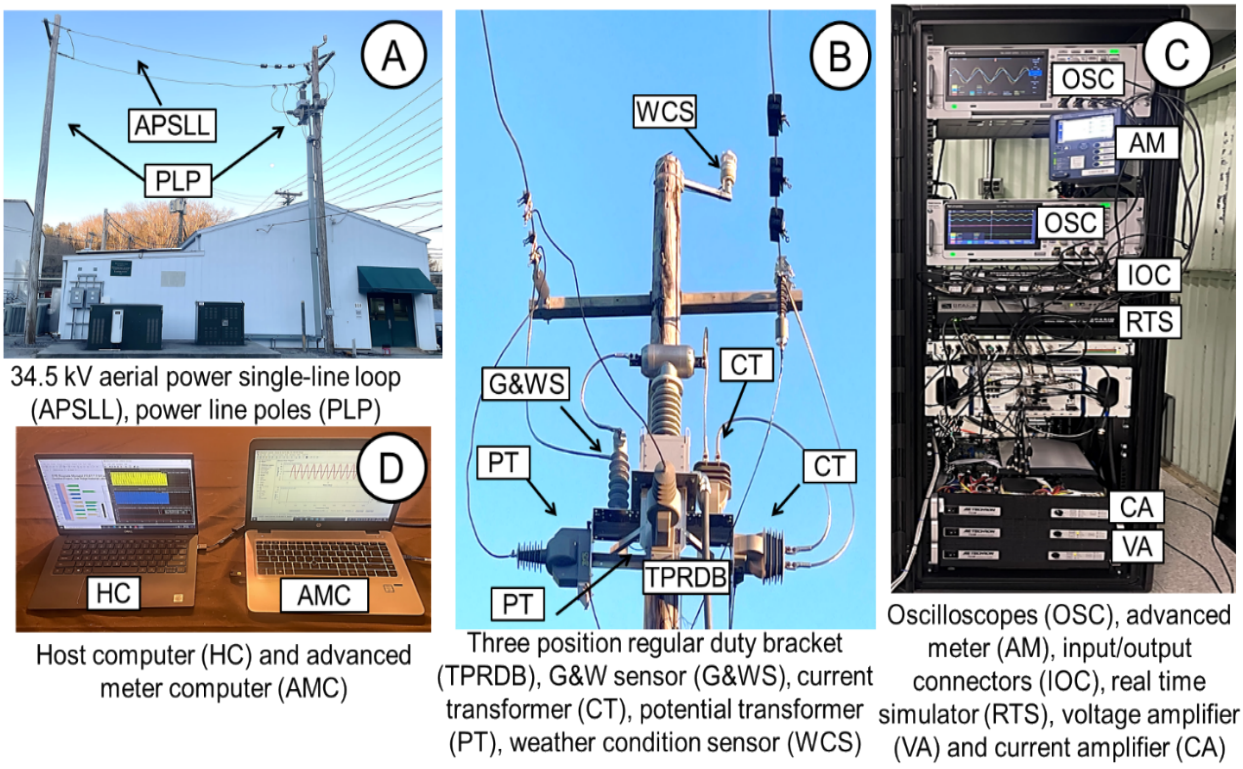

Figure 4. Medium-voltage aerial cable loop (A), power line pole with sensors (B), rack unit (C), and computers (D).

In the rack unit, the OP4510 real-time simulator generated the analog signals for the tests. These analog signals (up to 16 V) represented the power grid voltage and current signals that were connected to the electronic linear amplifiers to convert these analog signals into the voltage and current. Then, the voltage and current were fed into one PT/CT set to generate the primary voltage and current injected to the medium-voltage aerial cable loop. Then, the primary voltage and current were measured by another PT/CT set and the G&W power line sensor. In the medium-voltage OPLST, one PT/CT set was used as a voltage/current amplifier, and the second PT/CT set was used as a measurement device to compare

performance with the G&W power line sensor. At the computer desk (Figure 4D), the host computer run the real-time simulation tests at the OP4510 real-time simulator (target computer). There, part of the 12.4/7.2 kV EPB utility electrical grid was simulated. The OP4510 real-time simulator was connected to the host computer that ran the simulation tests based on different power grid scenarios such as electrical faults, capacitor bank and feeder switch operations. The power meter computer (Figure 4D) was used to set the SEL-735 power meter and collect the transient events as common format for transient data exchange (COMTRADE) files after running the tests. In the SEL-735 power meter, phase A was configured to measure the voltage/current of the simulated circuit or power grid, phase B measured the voltage/current signals of the PT/CT, and phase C measured the voltage/current signals of the G&W power line sensor.

3.7 SOFTWARE STEPS

The software steps for the medium-voltage OPLST were performed by using the MATLAB/Simulink, RT-LAB, AcSELerator Quickset, and SynchroWAVe software. The MATLAB/Simulink software was used to create the medium-voltage loop circuit and power grid models. The circuit was used to adjust the voltage/current gains for the OP4510 real-time simulator. The power grid simulated the 12.47 kV Riverside EPB utility circuit model to run the tests. The RT-LAB software was used to integrate these models with the OP4510 real-time simulator. The AcSELerator Quickset software was used to set the SEL-735 power meter, monitor the tests, and collect the test events as COMTRADE files. After running the tests, the SynchroWAVe software was used to plot and analyze the phase voltage/current signals from the test events. Figure 5 shows the software steps for the OPLST with the OP4510 real-time simulator and SEL-735 power meter.

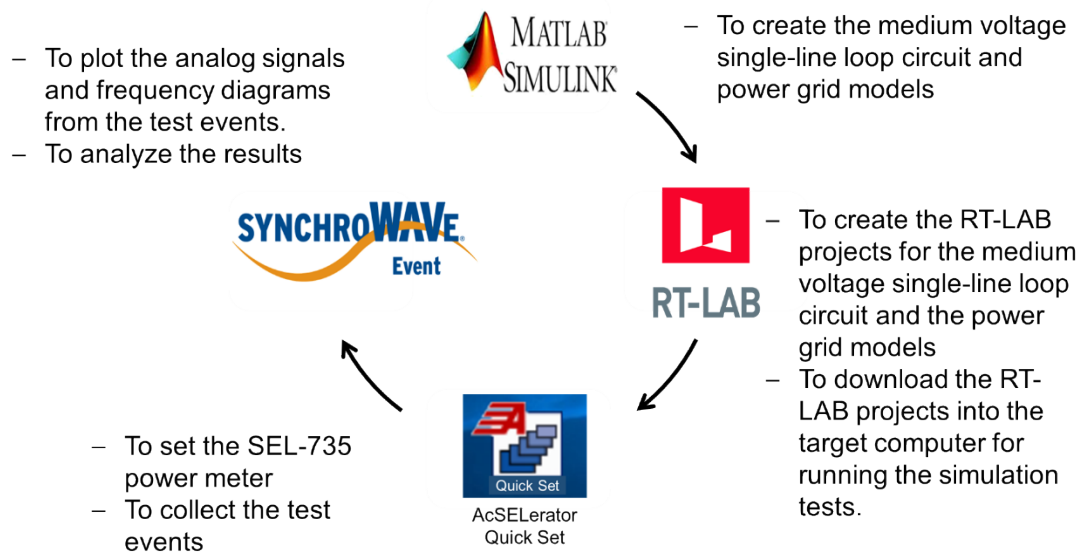

Figure 5. Software steps for the medium-voltage OPLST.

3.8 SEL-735 POWER METER WITH THE LOW-VOLTAGE INTERFACE

The SEL-735 power meter was used to measure the voltage/current signal of the power grid simulation, PT/CT, and G&W sensor. In Figure 6A, the rear side of the SEL-735 power meter on the rack unit is shown. The SEL-735 power meter can use the high-voltage/-current interface or low-voltage interface. For the high-voltage/-current interface, the PT/CT defined as reference devices were connected to phase B of the SEL-735 power meter, with a CT ratio of 80 and PT ratio of 175. For the low-voltage

interface, the phase voltage/current signal of the simulation, actual PT/CT signals, and actual G&W sensor signals were connected to phase A, B, and C, respectively. In the SEL-735 power meter, the low-voltage interface measured the voltage and current signals by a DB-25 connector that has a voltage scaling factor of 750 V/V and current scaling factor of 16.53 A/V. These voltage and current scaling factors were used to integrate the signals from the power grid simulation, PT/CT, and G&W sensor with the SEL-735 power meter through the OP4510 real-time simulator using Eqs. (13), (14), (15), (18), (19), and (20).

In Figure 6B, the Event Report Equations setting for the SEL-735 power meter is shown. The SEL-735 power meter can save the voltage/current signal events as COMTRADE files with 16, 128, and 512 samples per cycle [22]. The SEL-735 power meter was set with the AcSELerator Quickset software, and the event was triggered with the control input IN401 that was controlled with a signal of 16 Vdc (Pickup 15–30 Vdc) that was generated by the OP4510 real-time simulator. In the SEL-735 power meter, the waveform capture sample rate was set at 512 samples per cycle, and the event length was set at 300 cycles to record the test events for 5 s. The settings of the scaled signals were selected for the primary values (phase voltage and current at the medium-voltage aerial cable loop in the OPLST). In addition, the SEL-735 power meter has a color touchscreen that enabled observing the sinusoidal and phasor diagrams of voltage/current signals with 256 samples per cycle [22]. During the tests, the signals could be supervised from the display of the SEL-735 power meter practically in real time.

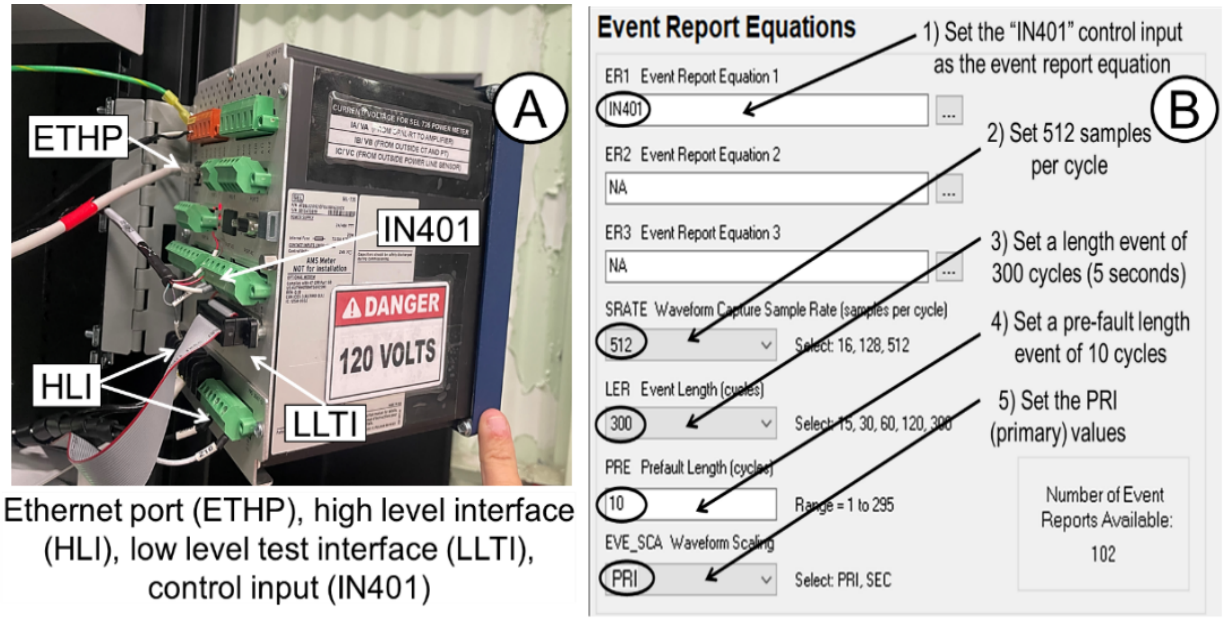

Figure 6. SEL-735 power meter rear side (A) and event report settings (B).

4. EXPERIMENTAL MODEL OF THE OPLST

In this section, the experimental model is presented. This design was based on comparing the performance of the G&W sensor power line sensor with the traditional PT/CT at the OPLST by using an OP4510 real-time simulator to create the voltage/current signals that represented part of the 12.47 kV Riverside EPB utility power grid. This experimental model was set for several test scenarios, such as different types of electrical faults, capacitor bank operation, and load fuse switch connections.

4.1 SINGLE-LINE DIAGRAM

In this study, the 12.47 kV Riverside EPB utility power grid model was used; the circuit was created with the MATLAB/Simulink software and integrated into an RT-LAB project to run with the OP4510 real-time simulator at the OPLST. Figure 7 shows the single-line diagram of the 12.47 kV Riverside Utility Grid (partial circuit).

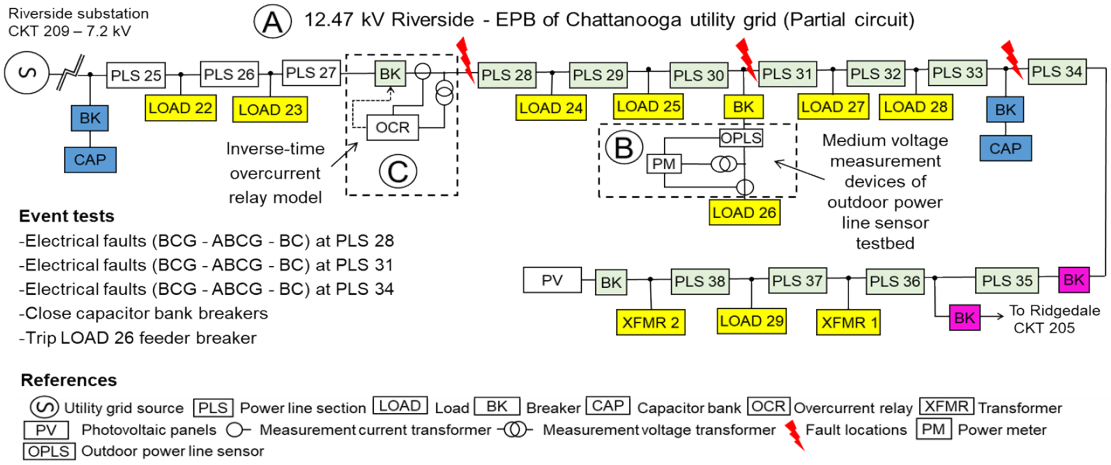

Figure 7. Single-line diagram of 12.47 kV Riverside EPB utility grid (partial circuit).

This network configuration is a radial power system (7.2 kV phase to ground voltage) that is fed by a three-phase source with a Wye-ground configuration (Figure 7A). At load 26 (Figure 7B), the voltage and current were measured by the G&W sensor and PT/CT at the load feeder. The overcurrent relay (Figure 7C) was located between power line sections 27 and 28 to clear the electrical faults along the power lines. In this experimental model, different tests were performed, such as the line to line ground (LLG), line to line (LL), and three-line to ground (3LG) electrical faults; capacitor bank operation; and load 26 fuse switch events.

4.2 RT-LAB PROJECT FOR THE REAL-TIME SIMULATOR

The 20/34.5 kV OPLST was run with the OP4510 real-time simulator. The SEL-735 power meter measured the voltage/current signals from the power grid, PT/CT, and G&W sensor. The RT-LAB project simulated the partial power grid of the 12.47 kV Riverside EPB utility created by the MATLAB/Simulink software. The RT-LAB project was formed by the SM_ Master and SC_Console subsystems, as shown in Figure 8. The RT-LAB project was set with a time step of 50 µs (powergui block) to simulate the test events. The SM_Master subsystem (Figure 8A) had the power grid and input/output interfaces. The SC_Console subsystem (Figure 8B) was used to supervise the tests with scopes that collected the measured voltage/current signals from the OP4510 real-time simulator, G&W power line sensor, and PT/CT.

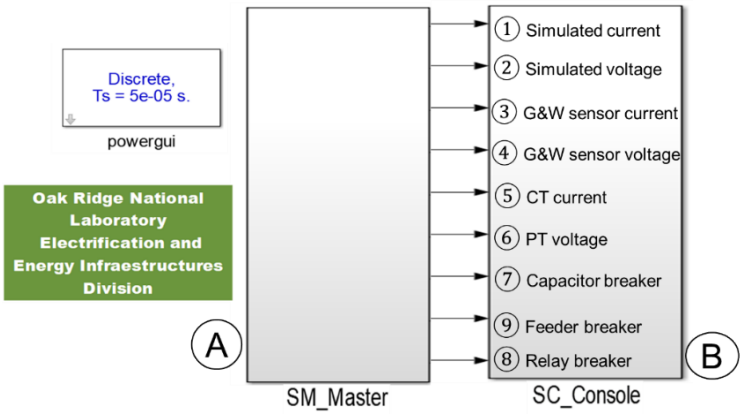

Figure 8. Subsystems of the RT-LAB project.

In the RT-LAB project, a partial power grid of the 12.47 kV Riverside EPB utility is shown in Figure 9. This power grid (Figure 9A) is represented by a three-line diagram circuit, relay breaker (Figure 9B), inverse time over-current relay (Figure 9C), fault block (Figure 9D), capacitor banks (Figure 9E), and feeder switch (Figure 9F). This power grid circuit includes the utility source, power line sections, feeder loads, breakers, and capacitor banks.

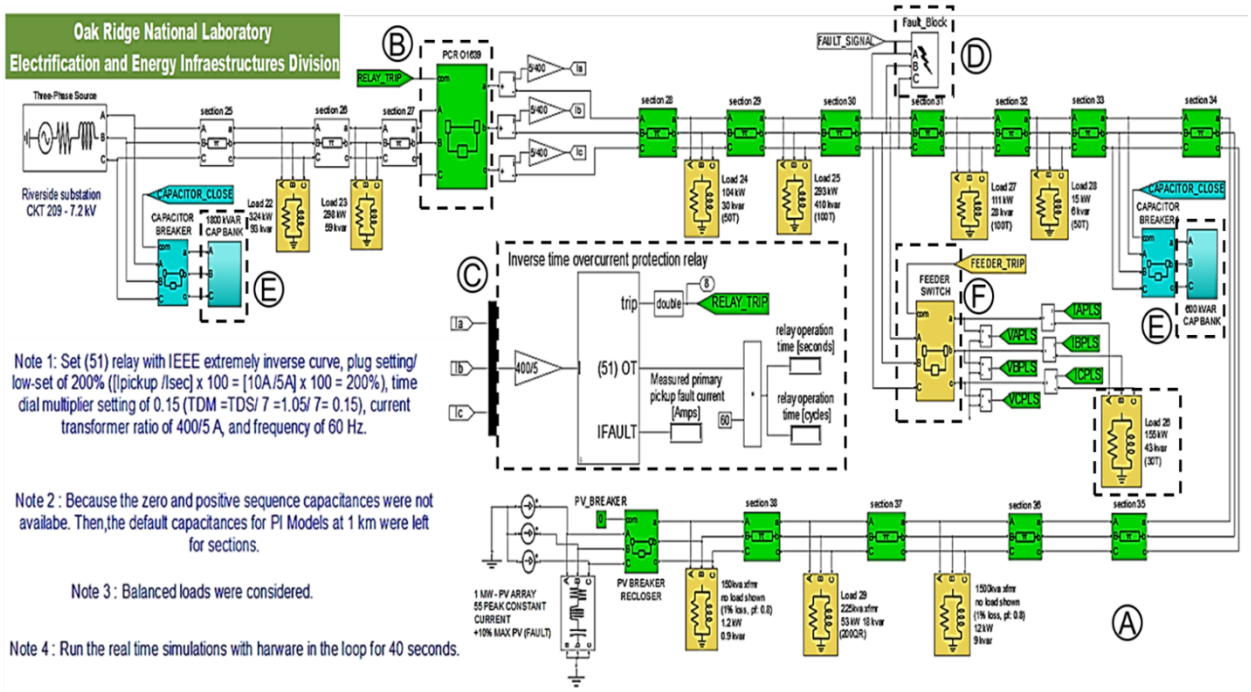

Figure 9. Three-line diagram of the power grid circuit (A), relay breaker (B), inverse time over-current relay (C), fault block (D), capacitor banks (E), and feeder switch (F).

In Figure 9, the power line sections were simulated with a three-phase π section line block. IntelliRupters are used in the 12.47 kV Riverside EPB utility grid [8], but an inverse time overcurrent relay MATLAB/Simulink model [23] was used on this study. The ratio of the CTs for the relay's breaker was 400/5 A. The inverse time over-current relay model (Figure 9C) was set with a time dial setting (*TDS*) of 1.05 s, CT ratio of 80, relay current pickup (*Ip*) of 10 A, and IEEE extremely inverse curve as shown in Eq. (23).

$$T_R = \frac{TDS}{7} \times \left(0.1217 + \frac{2.82}{\left(\frac{I_{primary}}{\frac{CTR}{I_p}} \right)^2 - 1} \right) \times 60 \,, \tag{23}$$

where T_R is the relay time in cycles and $I_{primary}$ is the primary current in amps.

The inverse-time over-current relay allowed for opening the breaker (Figure 9B) at the electrical fault currents. The grid simulation events were run to observe the pre-fault, fault, and post-fault states for each test. The simulated grid test events included the effect of the electrical fault resistance because the fault block (Figure 4D) was set with an electrical fault resistance of 0.001 ohms.

The OPLST was given by a medium-voltage aerial cable loop, so before running a test for the three-line diagram (Figure 9), the phase to be measured by the G&W power line sensor was selected from the phase setting circuit (Figure 10A), selecting 1, 2, or 3 for measuring phase A, B, or C, respectively.

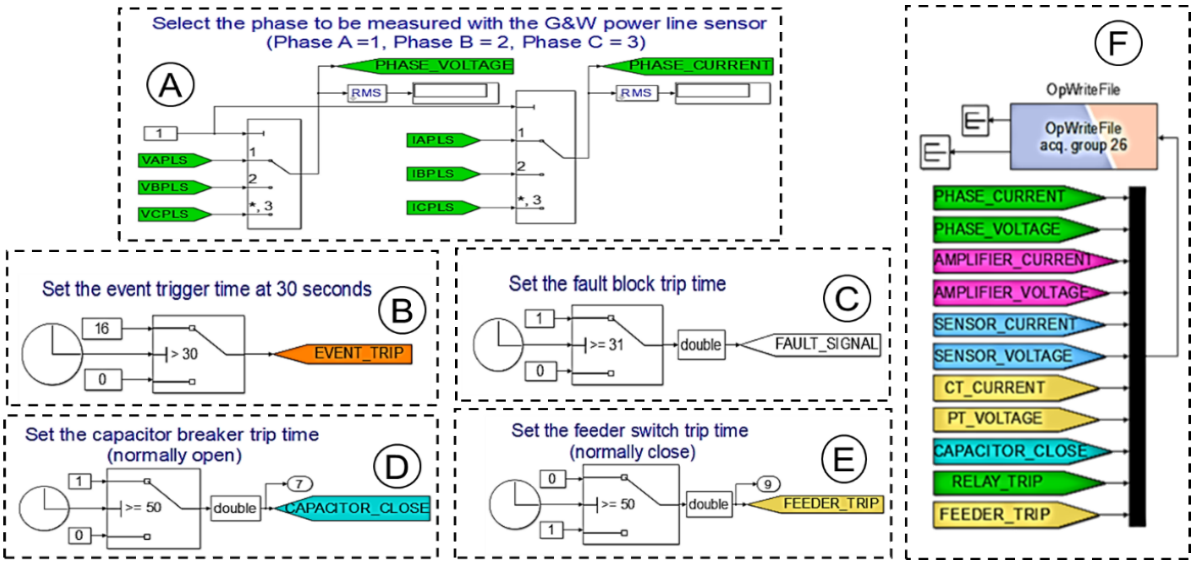

Figure 10. Phase setting circuit (A), event trigger circuit (B), electrical fault circuit (C), capacitor bank circuit (D), feeder switch circuit (E), and OpWrite File block (F).

During the tests, the real-time simulations were run for 40 s, and the signal to record the test event with the SEL-735 power meter was set at 30 s at the event trigger circuit (Figure 10B). To record the test event with the voltage/current signals before and after the transient events, the selected test scenario was tripped at 31 s, and the other test scenarios were set at 50 s.. Therefore, the electrical fault, capacitor bank, or feeder switch simulation test was selected. The electrical fault block circuit (Figure 10C) was set at 31 s, and the capacitor bank (Figure 10D) and feeder switch (Figure 10E) circuits were set at 50 s to run an electrical fault test by tripping the fault block (Figure 9D). The OpWrite File block (Figure 10F) allowed for collecting the test results as MATLAB files by saving the voltage/current signals from the G&W power line sensor, power grid, and PT/CT. Also, the capacitor bank and relay breaker states and feeder switch states were collected.

Figure 11 shows the interface circuits for the analog outputs and inputs of the OP4510 real-time simulator based on Figure 1B. The circuit for the event trip output signal for the SEL-735 power meter is shown in Figure 11A. The interface circuit for the voltage and current signals of the G&W OPLSs and PT/CT are

shown in Figure 11B. The analog outputs of the interface circuit for the gains of the OP4510 real-time simulator at the voltage/current amplifiers, PT/CT, and G&W OPLS are shown in Figure 11C.

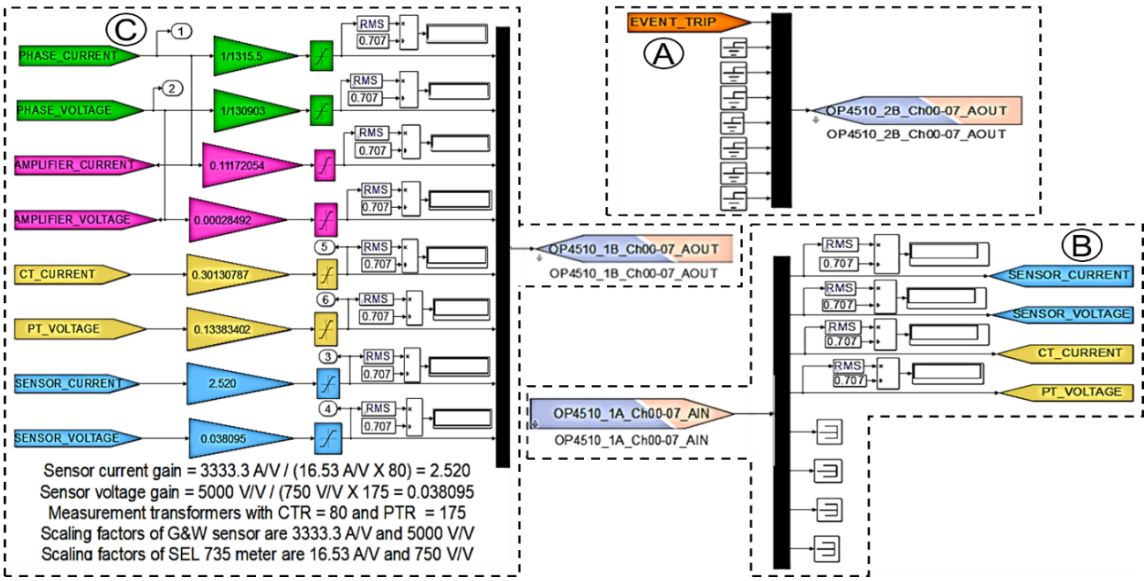

Figure 11. Event trip output signal (A), G&W and PT/CT input signals (B), and amplifier, PT/CT, and G&W sensor output signals (C).

Inside the SC_Console subsystem (Figure 8B) was set an Opcomm acquisition block (Figure 12) to collect the signals from the Master subsystem (Figure 8A). These signals were measured by three scopes to supervise the tests in real time. The breaker status and voltage/current signals of the simulated power grid (Figure 12A), G&W power line sensor (Figure 12B), and PT/CT (Figure 12C) were measured during the simulations.

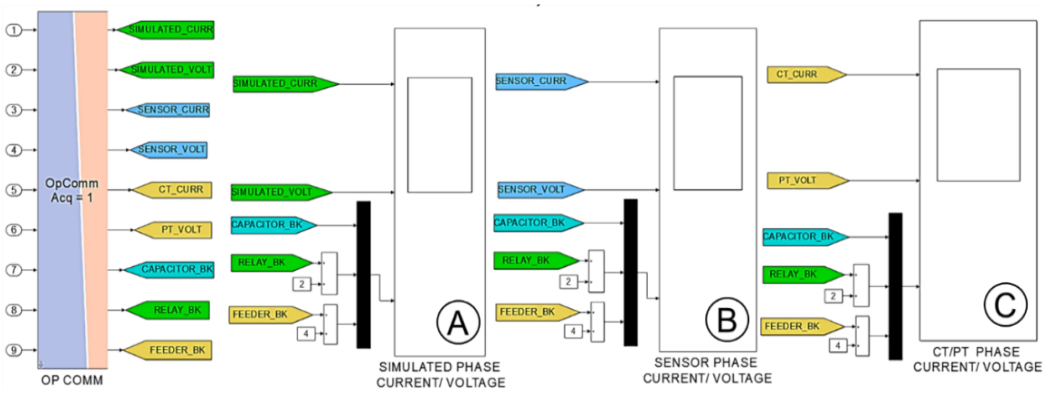

Figure 12. Scopes for the grid simulations (A), sensor (B), and PT/CT (C).

4.3 FLOWCHART FOR THE EXPERIMENTAL MODEL

The flowchart for the experimental model (Figure 13A) was based on the pre-test setting, simulation and data collection, and data plot and analysis. The tests were run with the OP4510 real-time simulator with a total simulation time of 40 s. The tests were recorded in the SEL-735 power meter at 30 s (Figure 10B) after starting the simulations, and the recorded data for all tests was 300 cycles (5 s). However, the data from the events were analyzed around the time when the electrical faults happened (i.e., when the breakers of feeders and capacitor banks were operated). This allowed for observation of the behavior of

phase voltage/current signals (Figure 13B and C) and harmonic analysis (Figure 13D and E) at transient events when comparing the performance of the G&W OPLS vs. the PT/CT.

In the experimental model (Figure 13A), the event trigger circuit was initially set to record the test events in the SEL-735 power meter at 30 s. Then, the type of test event was selected (electrical faults, capacitor bank, or feeder switch). If the electrical fault tests were selected, then the fault block was place on power line section 28, 31, or 34 (Figure 7), and the AB, ABG, or ABCG electrical faults were set on the fault block (Figure 9D). The fault block time was set at 31 s (Figure 10C) to generate the electrical fault, and the feeder switch and capacitor time blocks (Figure 10D and E) were set at 50 s. to not trip these scenarios during the simulation. If the capacitor bank test was selected, then the capacitor breaker time was set at 31 s (Figure 10D), and the electrical fault and feeder switch time blocks (Figure 10C and E) were set at 50 s. to not trip these scenarios at the tests. Finally, if the feeder switch test was selected, then the feeder switch breaker time was set at 31 s (Figure 10E), and the electrical fault and capacitor bank switch time blocks (Figure 10C and D) were set at 50 s. to not trip these scenarios at the tests.

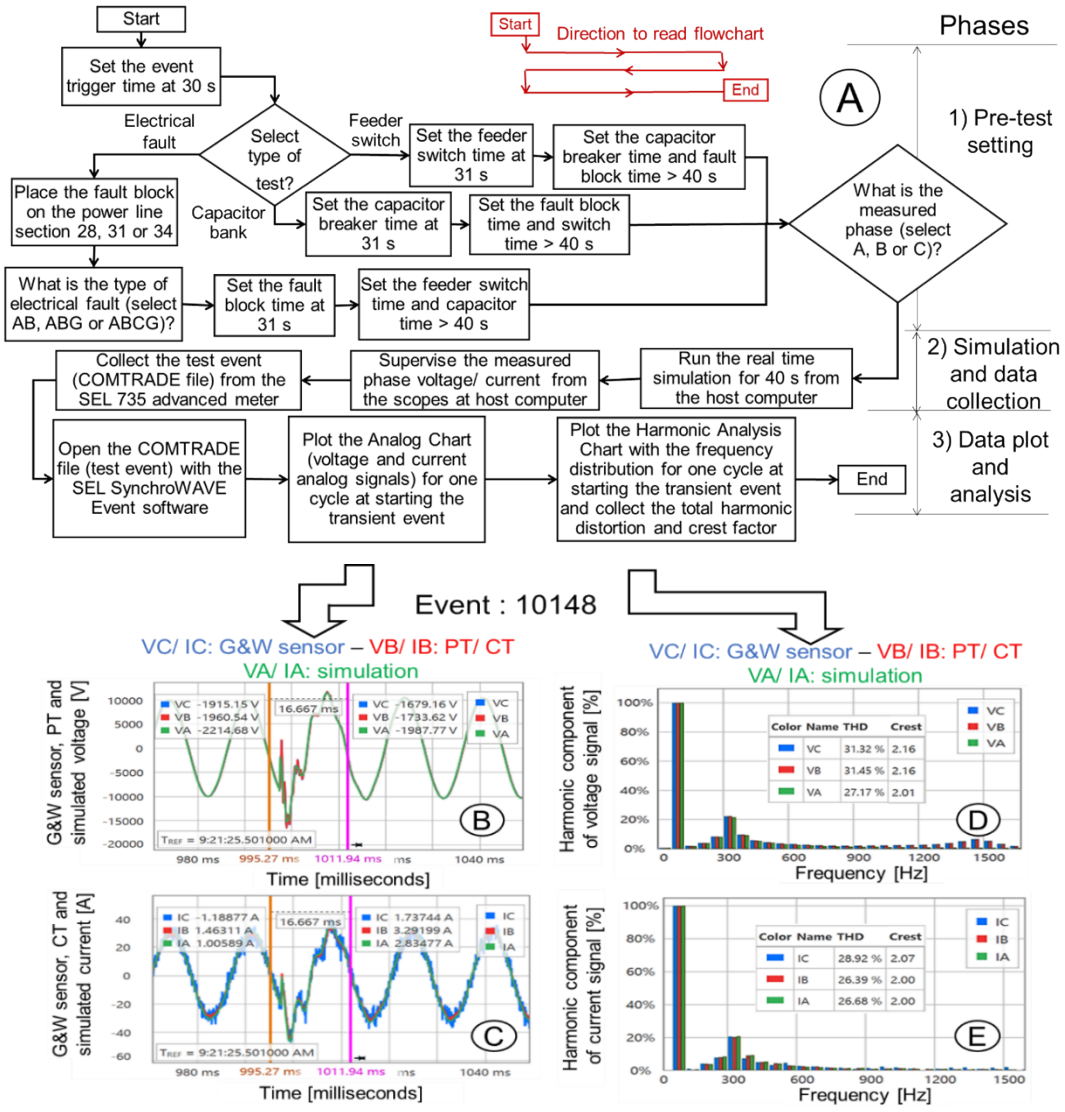

Figure 13. Flowchart to run the electrical fault, feeder switch, and capacitor bank tests with the OPLST using a real-time simulator and power meter.

In Figure 13A, once the electrical fault, capacitor bank, or feeder switch time blocks were set, the phase to be measured in the simulated power grid circuit (Figure 9) was selected by the phase setting circuit (Figure 10A) because the medium-voltage OPLST was based on a single-phase loop circuit (Figure 1). Then, the real-time simulation tests were run and supervised by the voltage/current scopes (Figure 12) from the host computer; the test events were collected from the SEL-735 power meter to plot the voltage/current signals on time domain (Figure 13B and C) and the harmonic components of voltage/current signals on frequency domain (Figure 13D and E), comparing the voltage/current signals from the simulated grid (phase A), PT/CT (phase B), and G&W OPLS (phase C).

5. RESULTS

In this section, the results for the electrical faults, capacitor bank operation, and load feeder switch event tests are presented. The total harmonic distortion and crest factor for voltage/current signals of phase A, B, and C were collected from the COMTRADE events. Then, the total harmonic distortion and crest factor percentage errors for the phase A, B, and C voltage/current signals from the G&W OPLS vs. the PT/CT were calculated.

5.1 TEST EVENTS AND RESULTS

The COMTRADE files for the electrical faults, capacitor bank operation, and feeder switch trip test events were collected and analyzed. Based on the experimental model (Figure 13), after each test was run, the COMTRADE file was collected, and the analog and frequency diagrams for the voltage/current signals were plotted. The voltage and current signals for the one-cycle (approx. 16.6 ms) transient state were observed in detail to compare the performance of the G&W power line sensor vs. the PT/CT. The total harmonic distortion and crest factor for the voltage/current signals of the G&W power line sensor and PT/CT were collected from the frequency plots. Then, the total harmonic distortion and crest factor percentage errors were calculated for the voltage/current signals. Table 4 lists the total harmonic distortion, crest factor, and percentage errors of the measured phase voltage/current signals from the G&W power line sensor vs. the PT/CT. The test events in Table 4 are shown in Appendix A, B, and C for measured phase A, B, and C, respectively.

In Table 4, the tests were named by the power grid measured phase (A, B, or C), type of load (load 26 multiplied by 3), type of event (electrical faults, capacitor bank operation, or feeder switch), and location. The total simulation time for each test was set at 40 s. The electrical fault (tests 1–3, 6–8, and 11–13), capacitor bank operation (tests 4, 9, and 14) and feeder switch (tests 5, 10, and 15) simulations were triggered at 31 s. The voltage and current signals from the PT/CT and G&W power line sensor on the load 26 feeder were recorded as COMTRADE files in the SEL-735 power meter. These COMTRADE file events had a total time of 5 s (300 cycles), capturing the voltage and current signals when the electrical faults, capacitor bank operation, or feeder switch test events were triggered.

The electrical fault tests were run for the LLG (phase B and C to ground), 3LG (phase A, B, and C to ground), and LL (phase B and C without ground) electrical faults. The BCG, ABCG, and BC electrical faults were set along the power line sections of the simulated power grid (Figures 7 and 9), but they were not set on the load 26 feeder (G&W power line sensor location). Then, the G&W power line sensor and PT/CT measured the distortion of voltage and current signals on the load 26 feeder when an electrical fault happened along the power line sections.

The OPLST accurately reproduced the current and voltage waveforms under most conditions but within limits because of the nature of the transformers operated under reverse conditions. The current amplifier that feeds the CT in the OPLST (Figure 1) cannot generate currents greater than 80 A in the aerial cable single-loop circuit without introducing distortions due to core nonlinearities. Thus, high-current faults could not be directly generated by the OPLST. Additionally, the PT used to step up the voltage has an intrinsic resonance at roughly 1,500 Hz, which became evident during events with abrupt voltage changes by a ringing of the applied voltage. The CT and PT used as reference sensors were extensively tested during the commissioning of the OPLST and found to be very accurate to beyond the 100th harmonic.

Table 4. Total harmonic distortion, crest factor, and percentage errors of the measured phase voltage and current from the G&W OPLS vs. the PT/CT

Test identification			Voltage total harmonic distortion factor (current total harmonic distortion factor)			Voltage crest factor (current crest factor)			G&W vs. PT (G&W vs. CT)	
Test number (event)	Test name[a,b]	Phase[c] (appendix)	G&W power line sensor	PT/CT sensor	Grid simulation	G&W power line sensor	PT/CT sensor	Grid simulation	Total harmonic distortion factor percentage error (%), Eqs. (7) and (8)	Crest factor percentage error (%), Eqs. (9) and (10)
1 (10139)	PHASE A_LOAD 26X3_BCG FAULT_SECTION 28 START	Phase A (Appendix A)	124.46 (193.13)	124.40 (159.57)	122.91 (160.93)	2.60 (3.86)	2.60 (3.58)	2.57 (3.70)	0.05 (21.03)	0.00 (7.82)
2 (10140)	PHASE A_LOAD 26X3_ABCG FAULT_SECTION 34 START		38.10 (66.14)	38.37) (53.78)	38.82 (55.71)	1.99 (2.26)	2.00) (2.02)	2.00 (1.98)	−0.70 (22.98)	−0.50 (11.88)
3 (10141)	PHASE A_LOAD 26X3_BC FAULT_SECTION 31 START		89.50 (94.57)	89.89 (84.70)	91.32 (86.28)	2.47 (2.76)	2.48 (2.47)	2.51 (2.44)	−0.43 (11.65)	−0.40 (11.74)
4 (10142)	PHASE A_LOAD 26X3_CLOSE BREAKER_ALL CAP BANKS		11.59 (17.56)	11.60 (11.48)	11.35 (11.50)	1.42 (1.75)	1.42 (1.51)	1.40 (1.51)	−0.09 (52.96)	0.00 (15.89)
5 (10143)	PHASE A_LOAD 26X3_OPEN SWITCH_30T FUSE FEEDER		161.95 (223.69)	162.61 (178.03)	162.43 (181.15)	3.18 (4.13)	3.21 (4.46)	3.14 (4.56)	−0.41 (25.65)	−0.93 (−7.40)
6 (10145)	PHASE B_LOAD 26X3_BCG FAULT_SECTION 28 START	Phase B (Appendix B)	266.90 (247.35)	268.77 (258.73)	230.88 (245.45)	2.81 (3.32)	2.78 (3.07)	3.39 (3.08)	−0.70 (−4.40)	1.08 (8.14)
7 (10146)	PHASE B_LOAD 26X3_ABCG FAULT_SECTION 34 START		169.91 (182.86)	170.47 (175.81)	138.02 (164.55)	3.06 (2.94)	3.04 (2.99)	3.62 (2.97)	−0.33 (4.01)	0.66 (−1.67)
8 (10147)	PHASE B_LOAD 26X3_BC FAULT_SECTION 31 START		87.07 (77.60)	87.62 (71.25)	71.08 (68.65)	2.07 (2.37)	2.05 (1.99)	2.28 (1.98)	−0.63 (8.91)	0.98 (19.10)
9 (10148)	PHASE B_LOAD 26X3_CLOSE BREAKER_ALL CAP BANKS		31.32 (28.92)	31.45 (26.39)	27.17 (26.68)	2.16 (2.07)	2.16 (2.00)	2.01 (2.00)	−0.41 (9.59)	0.00 (3.50)
10 (10149)	PHASE B_LOAD 26X3_OPEN SWITCH_30T FUSE FEEDER		125.89 (127.49)	126.15 (128.33)	128.78 (128.79)	3.14 (3.33)	3.15 (3.09)	3.19 (3.14)	−0.21 (−0.65)	−0.32 (7.77)

Test identification			Voltage total harmonic distortion factor (current total harmonic distortion factor)			Voltage crest factor (current crest factor)			G&W vs. PT (G&W vs. CT)	
Test number (event)	Test name[a,b]	Phase[c] (appendix)	G&W power line sensor	PT/CT sensor	Grid simulation	G&W power line sensor	PT/CT sensor	Grid simulation	Total harmonic distortion factor percentage error (%), Eqs. (7) and (8)	Crest factor percentage error (%), Eqs. (9) and (10)
11 (10150)	PHASE C_LOAD 26X3_BCG FAULT_SECTION 28 START	Phase C (Appendix C)	276.51 (254.08)	280.70 (230.95)	243.53 (237.88)	3.37 (3.42)	3.37 (3.48)	4.06 (3.53)	−1.49 (10.02)	0.00 (−1.72)
12 (10151)	PHASE C_LOAD 26X3_ABCG FAULT_SECTION 34 START		98.14 (86.91)	98.90 (85.22)	88.44 (86.65)	2.22 (2.78)	2.23 (2.52)	2.37 (2.47)	−0.77 (1.98)	−0.45 (10.32)
13 (10152)	PHASE C_LOAD 26X3_BC FAULT_SECTION 31 START		58.69 (45.84)	58.89 (40.50)	39.24 (37.09)	2.29 (3.09)	2.28 (2.59)	2.45 (2.62)	−0.34 (13.19)	0.44 (19.31)
14 (10153)	PHASE C_LOAD 26X3_CLOSE BREAKER_ALL CAP BANKS		32.03 (29.33)	32.18 (27.64)	27.95 (27.42)	1.71 (1.93)	1.71 (1.65)	1.64 (1.68)	−0.47 (6.11)	0.00 (16.97)
15 (10154)	PHASE C_LOAD 26X3_OPEN SWITCH_30T FUSE FEEDER		133.96 (146.97)	134.20 (134.90)	136.34 (134.99)	3.30 (3.60)	3.30 (3.35)	3.34 (3.40)	−0.18 (8.95)	0.00 (7.46)

[a]Test names (Measured phase and load_ Type of event and location). [b]The electrical fault, capacitor bank, and feeder switch tests were based on events with a time length of 300 cycles (5 s) that were analyzed at a 1-cycle transient state when the electrical fault happened, the capacitor bank breakers were closed, and the 30 T fuse feeder switch was opened. [c]A, B, or C phase of power grid feeder measured during the test in the OPLST.

6. DISCUSSION

The performance of the G&W power line sensor vs. the PT/CT was compared at the load feeder in the power grid circuit by using the OPLST with the OP4510 real-time simulator and SEL-735 power meter. The behavior of measured voltage and current signals from the G&W power line sensor vs. the PT/CT was studied and discussed for different test events (electrical faults, capacitor bank operation and load feeder switch). Analog and frequency plots from the COMTRADE event files were plotted for all tests to observe the behavior of voltage/current signals and harmonic components at the first one-cycle transient state of test events. Then, the total harmonic distortion and crest factor for the measured voltage and current signals of the G&W power line sensor and PT/CT were plotted and compared for phase A, B, and C of the power grid feeder.

6.1 ANALOG AND FREQUENCY PLOTS

The analog and frequency diagrams for the measured voltage and current signals of the COMTRADE file events from the test results were built with the SynchroWAVe software. The voltage/current analog and harmonic component plots of the G&W power line sensor, PT/CT, and simulated signals were plotted at three different phases and events. These plots were phase A of the load 26 feeder when the switch was opened (Figure 14), phase B for the power grid load 26 feeder with the ABCG electrical fault in power line section 38 (Figure 15), and phase C for the power grid load 26 feeder with all capacitor banks closed (Figure 16).

Figure 14 shows the analog signals (left) and harmonic components (right) that were collected from the SEL-735 power meter at the PHASE A_LOAD 26X3_OPEN SWITCH_30T FUSE FEEDER test. In Figure 14, the voltage, current, and harmonic components of the G&W power line sensor were phase A, the PT/CT was phase B, and the simulated power grid was phase C. The plots of Event 10143 (Figure 14) represent phase A of the load 26 feeder when the switch was opened (Figure 7). In this case, when the switch was opened, the voltage and current signals went from the nominal load values to zero (Figure 14A and B). The voltage and current signals from the G&W power line sensor (blue line) and PT/CT (red line) matched, demonstrating a good performance of the G&W power line sensor vs. the PT/CT. However, the G&W power line sensor current signal (blue line) had some noise that was practically constant during the test time (Figure 14B). The harmonic component plots for the voltage and current signals are shown in Figure 14C and D, respectively. In Figure 14C, the harmonic components of the voltage signal for the G&W power line sensor (blue bars) and PT (red bars) matched perfectly, demonstrating a good performance of the G&W power line sensor vs. the PT. In Figure 14D, the harmonic components of the current signal for the G&W power line sensor (blue bars) and CT (red bars) had a good match, too, but with different harmonic components for the G&W power line sensor (blue bars) after 600 Hz because of noise for the current signal (Figure 14B). The measured harmonic component for 60 Hz was 100% for the voltage (Figure 14C) and current (Figure 14D) signals.

Figure 15 shows the analog signal (left) and harmonic components (right) that were collected from the SEL-735 power meter at the PHASE B_LOAD 26X3_ABCG FAULT_SECTION 34 START test. In Figure 15, the voltage, current, and harmonic components of the G&W power line sensor were phase C, the PT/CT was phase B, and the simulated power grid was phase A. The plots of Event 10146 (Figure 15) represent phase B of the load 26 feeder when the ABCG electrical fault happened at power line section 34 (Figure 7). In this case, the voltage and current of the load 26 feeder decreased (Figure 15A and B) because the ABCG electrical fault point was grounded; most of the current went through the power line instead of the load 26 feeder, and the voltage decreased along the power line sections and consequently at the load 26 feeder (Figure 7). The voltage and current signals from the G&W power line sensor (blue line) and PT/CT (red line) matched well (Figure 15A and B), demonstrating a good performance of the G&W power line sensor vs. the PT/CT. In addition, the voltage signal of the G&W power line sensor

(blue line) and PT (red line) showed a ringing frequency during the transient (Figure 15A), and both kept the same path. In Figure 15B, the current signal of the G&W power line sensor (blue line) had some noise for that was practically constant during the test time. In Figure 15C, the harmonic components of the voltage signal for the G&W power line sensor (blue bars) and PT (red bars) matched perfectly, demonstrating a good performance of the G&W power line sensor vs. the PT. Also, the harmonic components of the voltage signal for the G&W power line sensor (blue bars) and PT (red bars) had similar percentage values for high frequencies (Figure 15C), which validated the ringing frequency of the voltage signal during the transient (Figure 15A) for the G&W power line sensor and PT. In Figure 15D, the harmonic component of the current signal for the G&W power line sensor (blue bars) and CT (red bars) had a good match, too, but with different harmonic components for the G&W power line sensor (blue bars) because of the noise for the current signal (Figure 15B). The measured harmonic component for 60 Hz was 100% for the voltage (Figure 15C) and current (Figure 15D) signals.

Figure 16 shows the analog signals (left) and harmonic component (right) plots that were collected from the SEL-735 power meter at the PHASE C_LOAD 26X3_CLOSE BREAKER_ALL CAP BANKS test. In Figure 16, the voltage, current, and harmonic components of the G&W power line sensor were phase C, the PT/CT was phase B, and the simulated power grid was phase A. The plots of Event 10153 (Figure 16) represent phase C of the load 26 feeder when capacitor banks are closed (Figure 7). In this case, the voltage and current signals of the load 26 feeder were distorted during the transient (Figure 16A and B) because the capacitor banks were connected near the load 26 feeder (Figure 7). The voltage and current signals from the G&W power line sensor (blue line) and PT/CT (red line) matched, demonstrating a good performance of the G&W power line sensor vs. the PT/CT. Also, the voltage and current signals of the G&W power line sensor (blue lines) and PT/CT (red lines) experienced a distortion during the transients (Figure 16A and B), and both kept the same path. In Figure 16B, the current signal of the G&W power line sensor (blue line) had a little noise that was practically constant during the test time. The harmonic components of the voltage (Figure 16C) and current (Figure 16D) signals for the G&W power line sensor (blue bars) and PT (red bars) matched perfectly, demonstrating a good performance of the G&W power line sensor vs. the PT. The measured harmonic component for 60 Hz was 100% for the voltage (Figure 16C) and current (Figure 16D) signals.

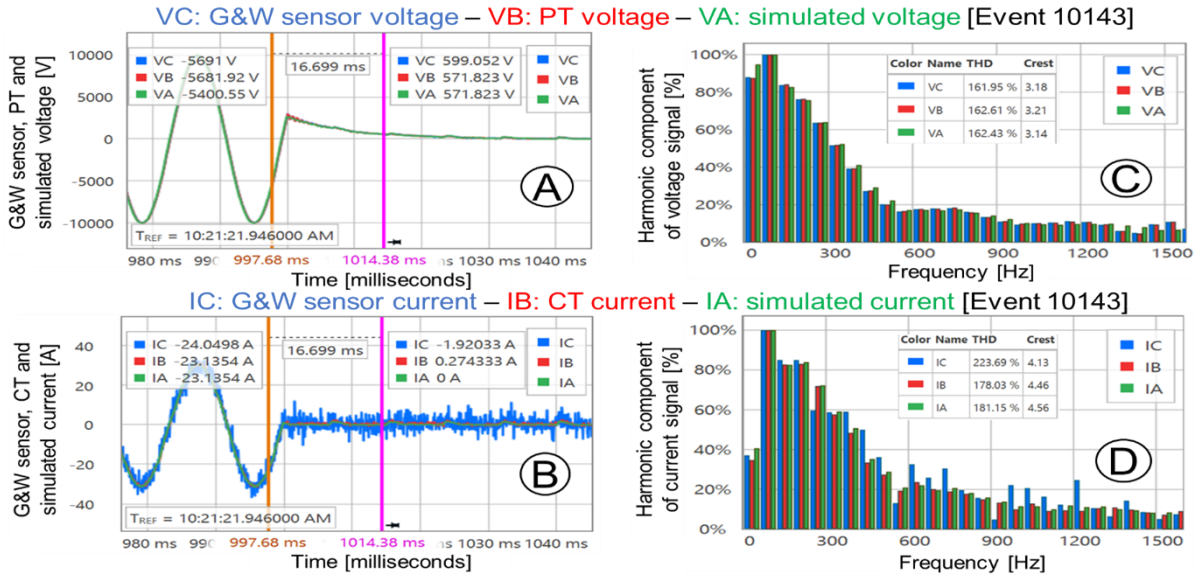

Figure 14. Analog (A, B) and harmonic (C, D) plots of the G&W sensor, PT/CT, and simulated signals at phase A of the load 26 feeder when the switch was opened.

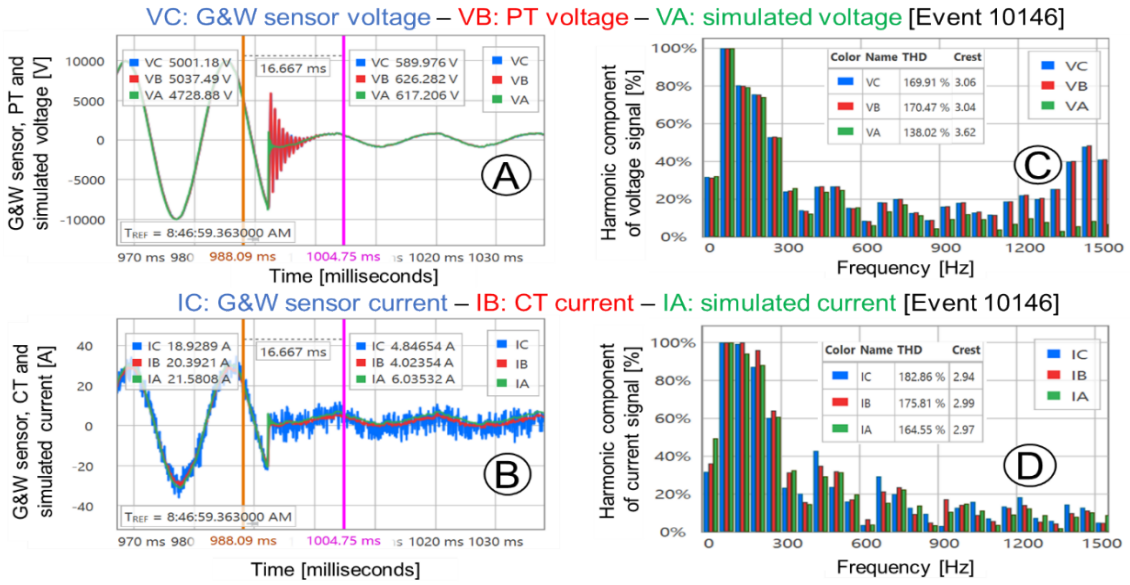

Figure 15. Analog (A, B) and harmonic (C, D) plots of the G&W sensor, PT/CT, and simulated signals at phase B for the load 26 feeder with ABCG electrical fault in power line section 38.

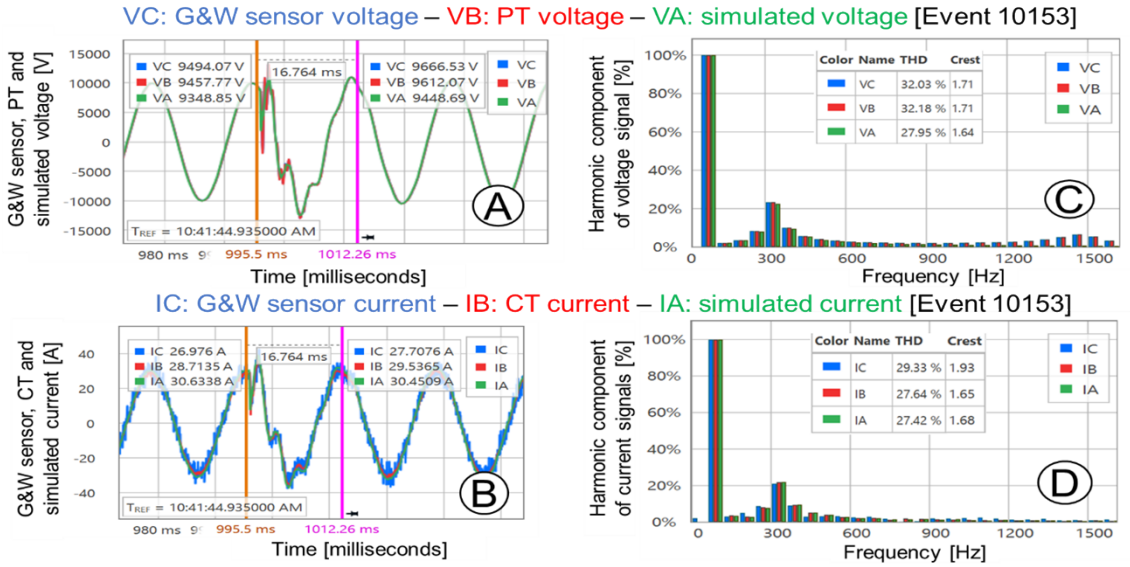

Figure 16. Analog (A, B) and harmonic (C, D) plots of the G&W sensor, PT/CT, and simulated signals at phase C for the load 26 feeder with all capacitor banks closed.

6.2 TOTAL HARMONIC DISTORTION AND CREST FACTOR

The total harmonic distortion of test events (electrical faults, capacitor bank operators, and load feeder switch) for the measured phase A, B, and C voltage (Figure 17A) and current (Figure 17B) signals in the power grid feeder were plotted, comparing the performance of the PT/CT and G&W power line sensor. The total harmonic distortions were collected from the frequency plots built by the COMTRADE files from the test results (Table 4). In Figure 17, the total harmonic distortions are represented by the green solid lines (voltage and current signals from the simulated power grid feeder), red dashed lines (voltage and current signals from the PT/CT), and blue dotted lines (voltage and current signals from the G&W

power line sensor). The total harmonic distortion for the measured voltage (Figure 17A) and current (Figure 17B) signals of the G&W power line sensor and PT showed a similar performance for the electrical faults, capacitor bank, and load feeder switch test events, as shown from the red dashed lines and blue dotted lines having similar paths, but the performance was better for voltage signals than current signals.

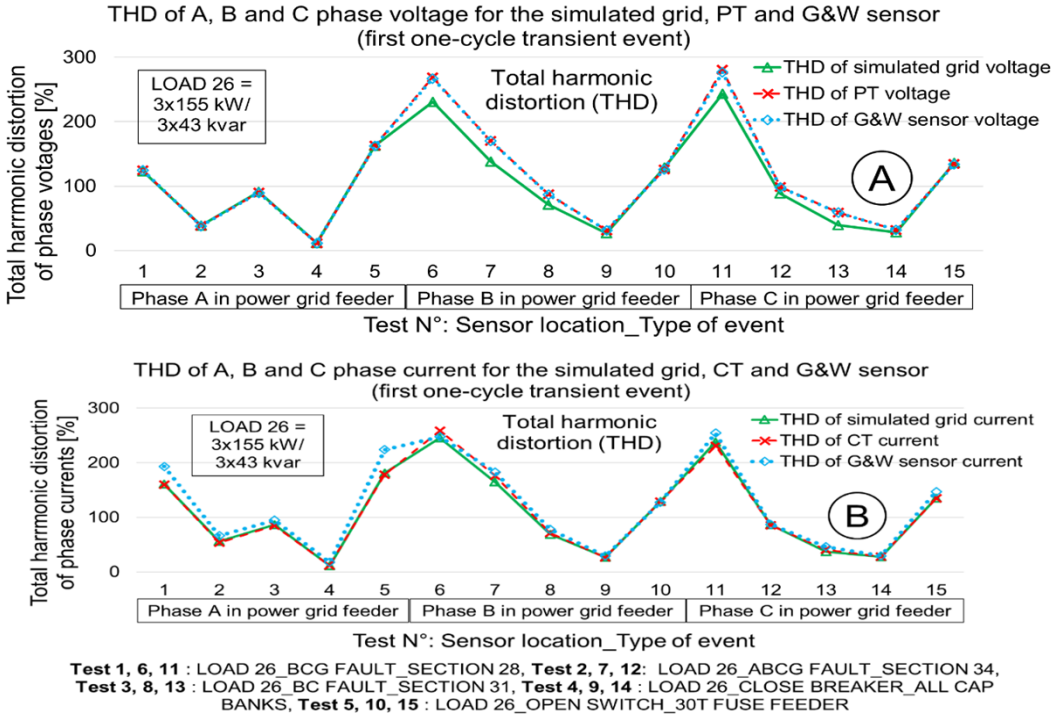

Figure 17. Total harmonic distortion of phase A, B, and C voltage (A) and current (B) signals for the simulated grid, PT/CT, and G&W sensor.

The crest factors of test events (electrical faults, capacitor bank operators, and load feeder switch) for the measured phase A, B, and C voltage (Figure 18A) and current (Figure 18B) signals in the power grid feeder were plotted, comparing the performance of the PT/CT and G&W power line sensor. The crest factors were collected from the harmonic analysis built by the COMTRADE files from the test results (Table 4). In Figure 18, the crest factors are represented by the green solid lines (voltage and current signals from the simulated power grid feeder), red dashed lines (voltage and current signals from the PT/CT), and blue dotted lines (voltage and current signals from the G&W power line sensor). The crest factors for the measured voltage (Figure 18A) and current (Figure 18B) signals of the G&W power line sensor and PT had similar performance for the electrical faults, capacitor bank, and load feeder switch test events, as shown from the red dashed lines and blue dotted lines having similar paths, but the performance was better for voltage signals than current signals.

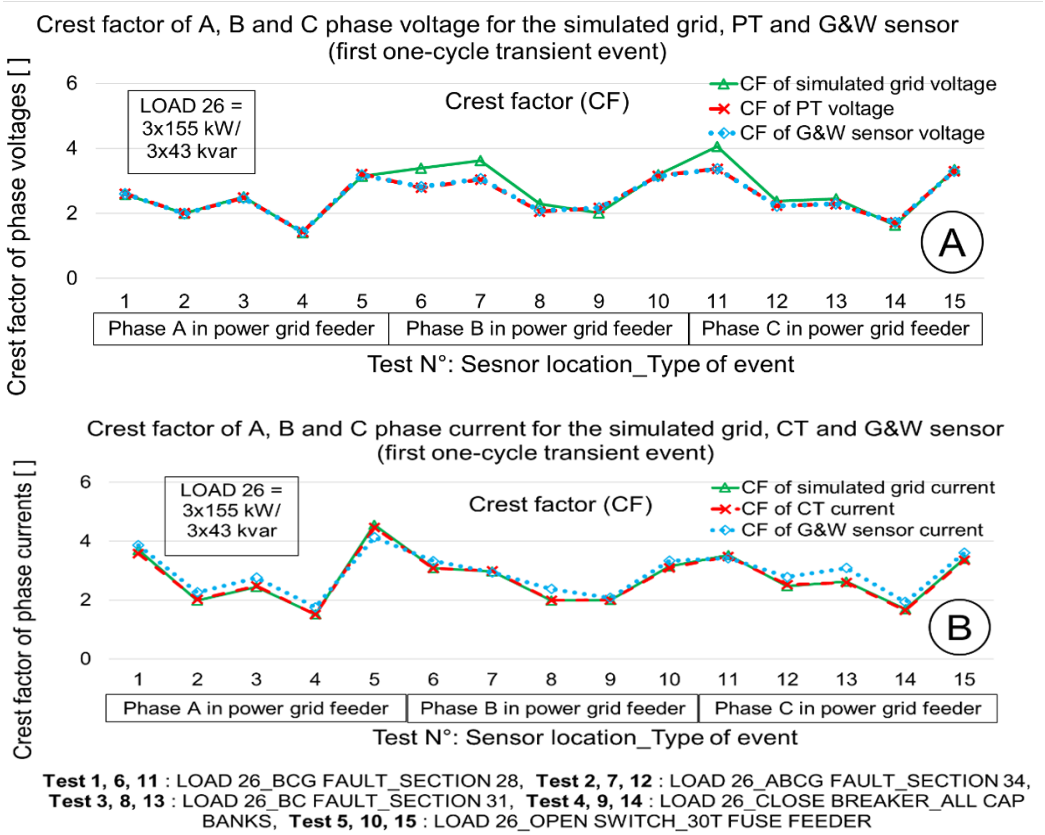

Figure 18. Crest factor of phase A, B, and C voltage (A) and current (B) signals for the simulated grid, PT/CT, and G&W sensor.

6.3 TOTAL HARMONIC DISTORTION AND CREST FACTOR PERCENTAGE ERRORS

The total harmonic distortion and crest factor percentage errors of test events (electrical faults, capacitor bank operators, and load feeder switch) for the measured phase A, B, and C voltage (Figure 19A) and current (Figure 19B) signals in the power grid feeder were plotted, comparing the performance of the G&W power line sensor vs. the PT/CT. In Figure 19, the percentage errors for the total harmonic distortion and crest factor values correspond to the first one-cycle transient event for the simulated tests. The total harmonic distortion and crest factor percentage errors were calculated by Eqs. (7), (8), (9), and (10), as described in Table 4. For the calculation of the percentage errors, the signals from the PT/CT and the G&W power line sensor were considered as the expected and measured values, respectively. In Figure 19A, the pink bars are the total harmonic distortion (0.05% to −1.49%) of the voltage signals, and the blue bars are the crest factor (1.08% to −0.93%) percentage errors of the voltage signals. In Figure 19B, the green bars are the total harmonic distortion (52.96% to −4.40%) percentage errors of the current signals, and the red bars represent the crest factor (19.31% to −7.4%) percentage errors of the current signals.

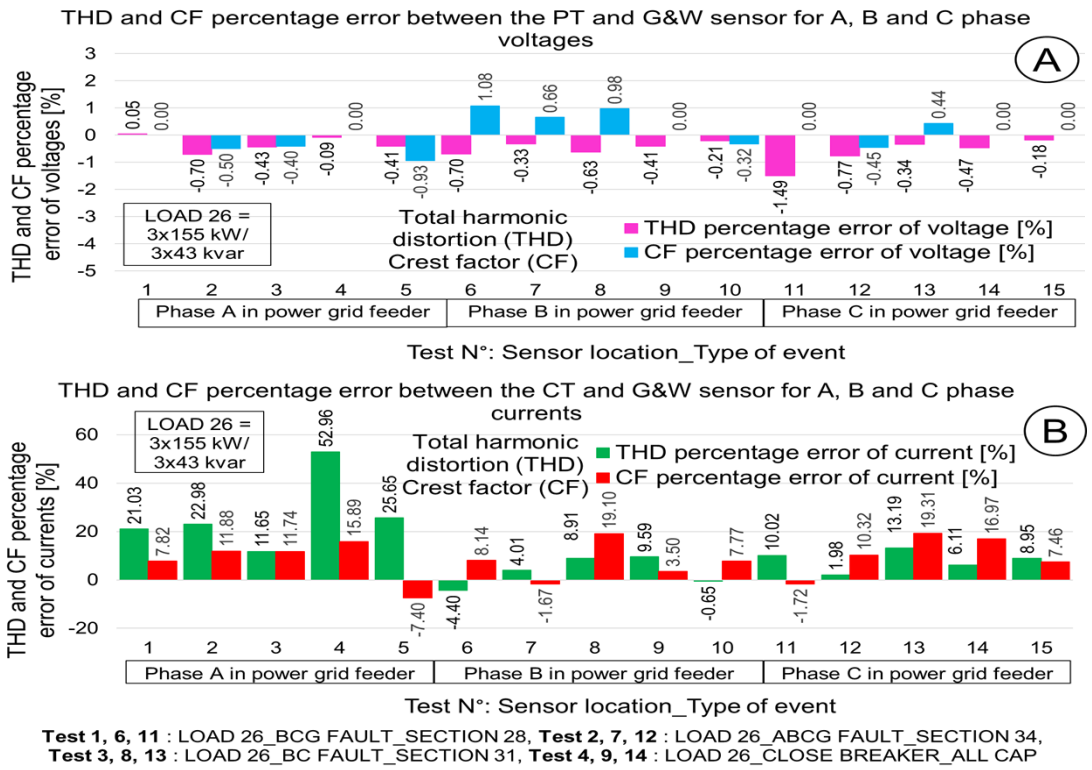

Figure 19. Total harmonic distortion and crest factor percentage error of phase A, B, and C for the voltage (A) and current (B) signals between the G&W sensor and the PT/CT.

6.4 ANALOG SIGNAL PLOTS AND VOLTAGE/CURRENT INCEPTION ANGLES

In the electrical fault events, the inception time is the moment at which the electrical fault is initiated. The fault inception angle is defined by the voltage phasor (angle) as a ground electrical fault is initiated. Therefore, different fault inception angles can be observed by varying the time when the electrical fault is initiated. Thus, the fault inception angles can generate different transient events for the phase voltage or current signals [24], and consequently also different transient events. The test events (electrical faults, capacitor bank operation, and load feeder switch) were run for phase A, B, and C. These showed different voltage and current signal behaviors for transient states because the experimental model (Figure 13A) was designed to measure phase A, B, and C in the power grid feeder at the medium-voltage OPLST (Figure 1). Since the test events were triggered at the same time, the measured phase A, B, and C current and voltage signals generated different inception angles based on a three-phase system definition [25].

In the capacitor bank operation tests (Events 10142, 10148 and 10153), the effect of the fault inception angles for the voltage and current signals was observed by plotting the first one-cycle transient event at the measured phase A, B, and C. These events represent the time when the capacitor banks along the power line sections were closed in the simulated power grid (Figure 7). The voltage and current signals at the load feeder (Figure 7B) were measured at the medium-voltage OPLST. The measured voltage (Figure 20A, B, and C) and current (Figure 20D, E, and F) signals for phase A, B, and C were compared for the G&W power line sensor vs. the PT/CT. In Figure 20, the blue, red, and green lines are the voltage/current signals for the G&W power line sensor, PT/CT, and simulated power grid, respectively. For the first one-cycle transient event (approx. 16.6 ms), the behavior of the voltage and current signals for the G&W power line sensor and PT/CT were similar for the same measured phase. However, the transient voltage and current signals for phase A (Figure 20A and D), B (Figure 20B and E), and C (Figure 20C and F) had different shapes because the tests were tripped at the same time, but phase A, B,

and C reached their instantaneous peak values at different times based on a three-phase system definition [25].

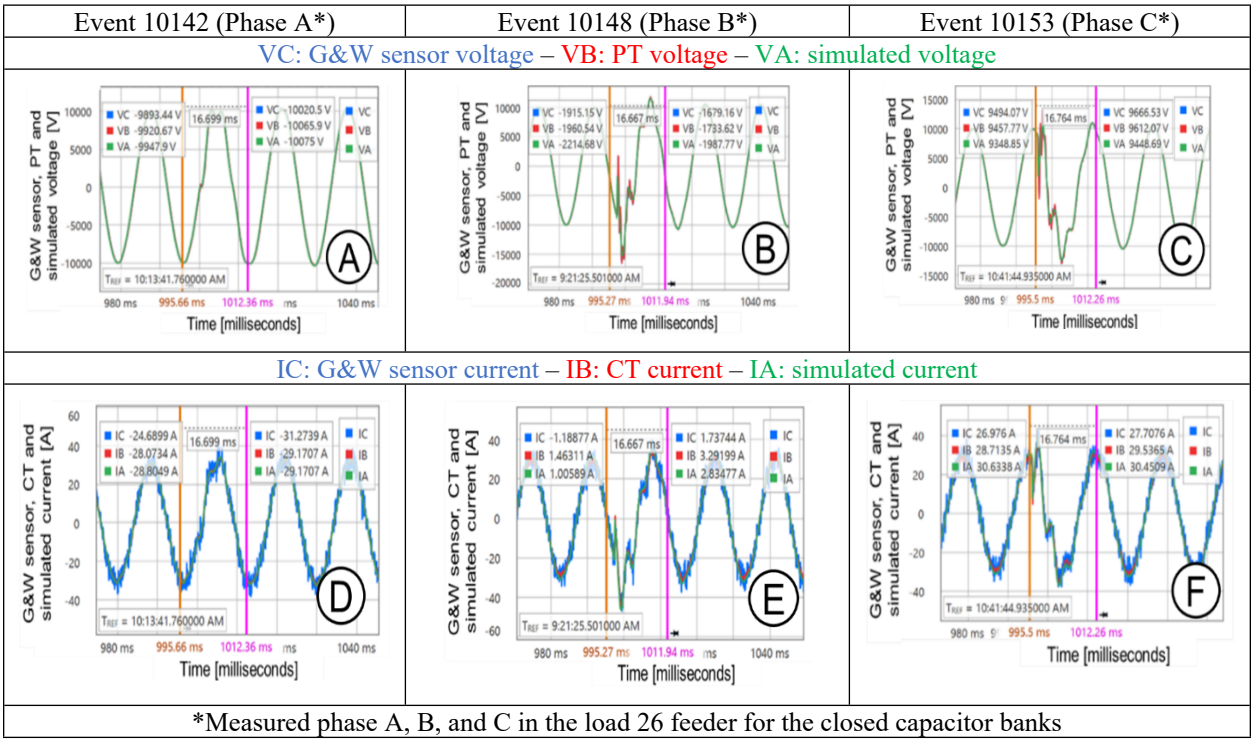

Figure 20. Voltage and current of phase A (A, D), B (B, E), and C (C, F) for the G&W power line sensor, PT/CT, and simulated power grid at the load 26 feeder when the capacitor banks are closed.

In the ABCG electrical fault event tests (Events 10140, 10146, and 10151), the effects of the fault inception angles for the voltage signals were plotted for the first one-cycle transient event at phase A, B, and C. These events represent the time when the electrical fault happened at power line section 34 in the simulated power grid (Figure 7). Then, the voltage and current signals at the load feeder (Figure 7B) were generated at the medium-voltage OPLST. The effect of the ABCG electrical fault at the power line produced the phase currents and voltages decreased on the load feeder (Figure 21). The measured voltage (Figure 21A, B, and C) and current (Figure 21D, E, and F) signals for phase A, B, and C were compared with the G&W power line sensor vs. the PT/CT. In Figure 21, the blue, red, and green lines are the voltage/current signals for the G&W power line sensor, PT/CT, and simulated power grid, respectively. For the first one-cycle transient event (approx. 16.6 ms), the behavior of the voltage and current signals for the G&W power line sensor and PT/CT were similar for the same measured phase. However, the transient voltage and current signals for phase A (Figure 21A and D), B (Figure 21B and E), and C (Figure 21C and F) had different shapes because the tests were tripped at the same time, but phase A, B, and C reached their instantaneous peak values at different times based on a three-phase system definition [25]. Therefore, the voltage and current inception angles for phase A (Figure 21A and D), B (Figure 21B and E), and C (Figure 21C and E) were different. In the first one-cycle transient event, the voltage and current signals of phase A had shown a sinusoidal (Figure 21A and D), whereas the voltage signals of phase B and C had a distortion (Figure 21B and C) that generated a ringing frequency for the G&W power line sensor and PT. In addition, the current signals of phase A, B, and C (Figure 21D, E, and F) had different shapes because their inception angles were different, as well.

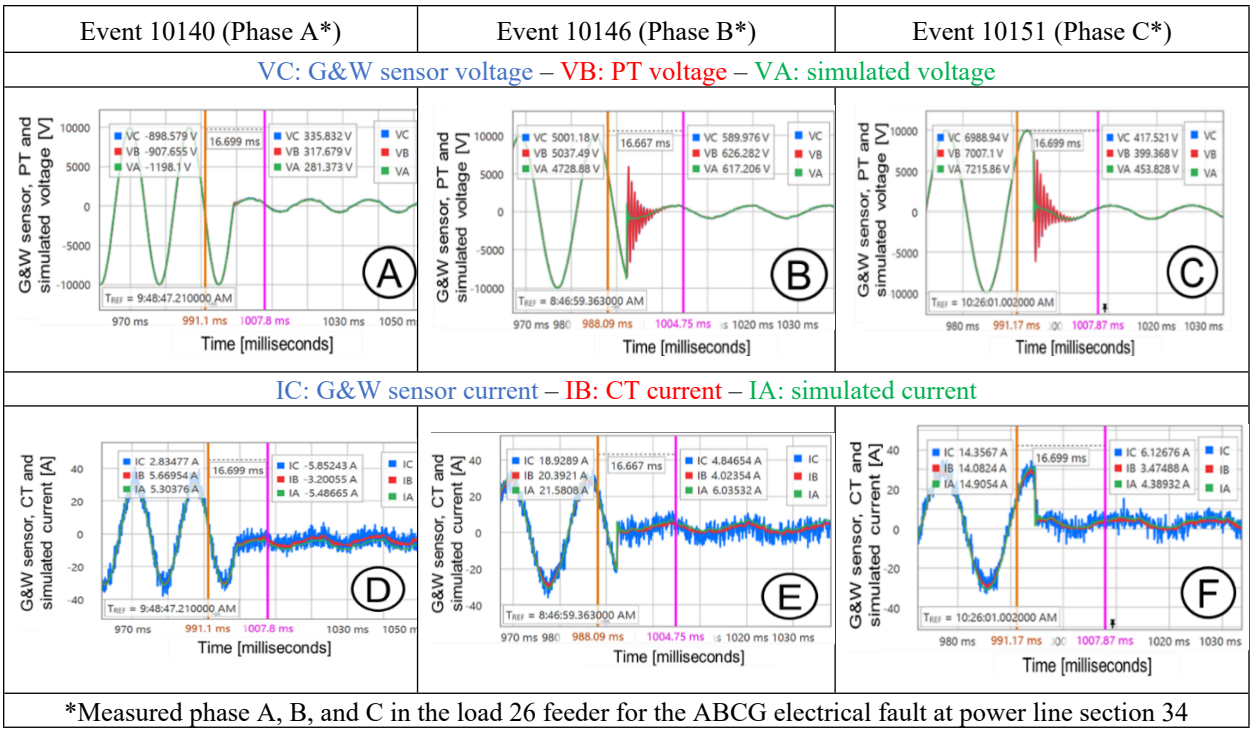

Figure 21. Voltage and current of phase A (A, D), B (B, E), and C (C, F) for the G&W power line sensor, PT/CT, and simulated power grid at the load 26 feeder and ABCG electrical fault in power line section 34.

6.5 FREQUENCY ANALYSIS FOR VOLTAGES AND CURRENTS

The simulated power grid (Figure 9) has a fundamental frequency of 60 Hz, but during the one-cycle transient events (approx. 16.6 ms) for the electrical fault test events, other frequencies could be measured because of distortion of the voltage and current signals. The voltage harmonic components (Figure 22A, B, and C) and corresponding voltage signals (Figure 22D, E, and F) for the G&W power line sensor, PT/CT, and simulated power grid at the load 26 feeder and BC electrical fault in power line section 31 are shown from Events 10141 (phase A), 10147 (phase B), and 10152 (phase C). The measured harmonic components of voltage signals for phase A (Figure 22A), B (Figure 22B), and C (Figure 22C) were plotted for a one-cycle transient event (approx. 16.6 ms). The harmonic components of voltage signals for the G&W power line sensor (blue bars) and PT (red bars) had similar behavior. In Figure 22A, B, and C, the greatest harmonic component of voltage signals was at 60 Hz for phase A, B, and C. Also, the harmonic components of voltage signals at 0 Hz were smaller than at 60 Hz because the test event was given by a BC (non-grounding) electrical fault. In Figure 22B and C, the G&W power line sensor (blue bars) and PT (red bars) harmonic components of the voltage signals matched at high frequencies because of the ringing voltage behavior in Figure 22E and F.

The measured harmonic components of current signals (Figure 23A, B, and C) and current signals (Figure 23D, E, and F) for the G&W power line sensor, PT/CT, and simulated power grid at the load 26 feeder and the BC electrical fault in power line section 31 are shown from Events 10141 (phase A), 10147 (phase B), and 10152 (phase C). The measured harmonic components of current signals for phase A (Figure 23A), B (Figure 23B), and C (Figure 23C) were plotted for a one-cycle transient event (approx. 16.6 ms). The harmonic components of current signals for the G&W power line sensor (blue bars) and PT (red bars) had similar behavior. The greatest harmonic component of current signal was at 60 Hz for phase A, B, and C (Figure 23A, B, and C). Also, the harmonic components of current signals at 0 Hz were smaller than at 60 Hz because the test was given by a BC (non-grounding) electrical fault. In

Figure 23A, B, and C, the harmonic components of current signals for the G&W power line sensor (blue bars) and CT (red bars) were almost matched, with a slight difference in their harmonic components because of the minor noise of the current signals (Figure 23D, E, and F).

Event 10141 (Phase A*)	Event 10147 (Phase B*)	Event 10152 (Phase C*)
VC: G&W sensor voltage – VB: PT voltage – VA: simulated voltage		
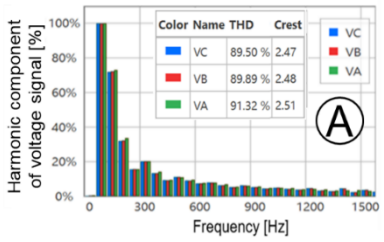	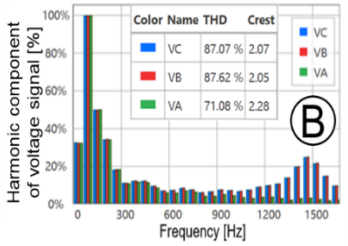	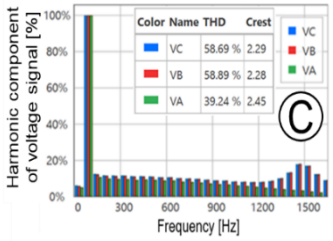
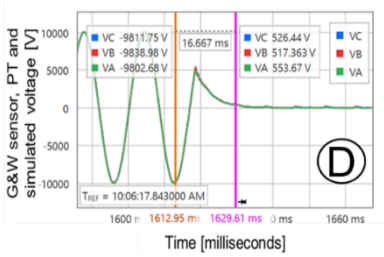	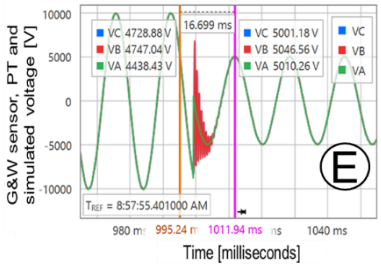	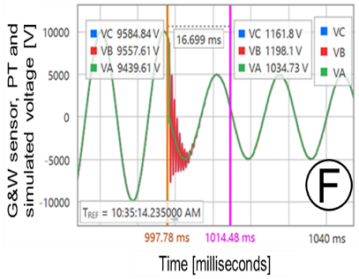
*Measured phase A, B, and C voltages in the load 26 feeder for the BC electrical fault at power line section 31		

Figure 22. Phase A, B, and C voltage harmonic components (A, B, C) and voltage signals (D, E, F) for the G&W power line sensor, PT/CT, and simulated power grid at the load 26 feeder and BC electrical fault in power line section 31.

Event 10141 (Phase A*)	Event 10147 (Phase B*)	Event 10152 (Phase C*)
IC: G&W sensor current – IB: CT current – IA: simulated current		
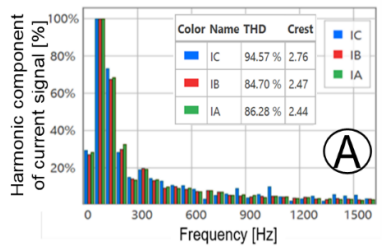	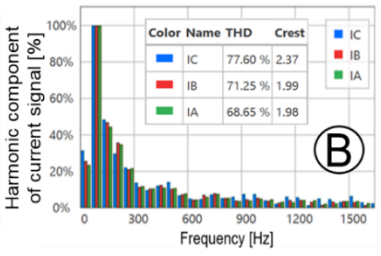	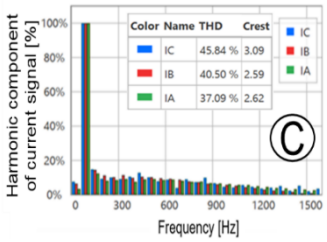
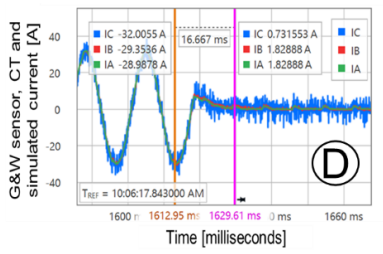	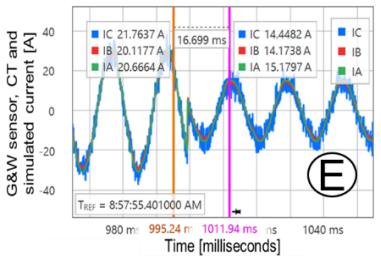	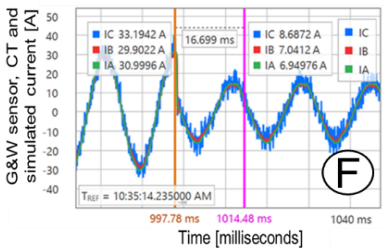
*Measured phase A, B, and C currents in the load 26 feeder for the BC electrical fault at power line section 31		

Figure 23. Phase A, B, and C current harmonic components (A, B, C) and current signals (D, E, F) for the G&W power line sensor, PT/CT, and simulated power grid at the load 26 feeder and BC electrical fault in power line section 31.

The measured harmonic components of voltage signals (Figure 24A, B, and C) and voltage signals (Figure 24D, E, and F) for the G&W power line sensor, PT/CT, and simulated power grid at the load 26 feeder and the ABCG electrical fault in power line section 34 are shown from Events 10140 (phase A), 10146 (phase B), and 10151 (phase C). The measured harmonic components of voltage signals for the phase A (Figure 24A), B (Figure 24B), and C (Figure 24C) were plotted for a one-cycle transient event (approx. 16.6 ms). In Figure 24A, B, and C, the harmonic components of voltage signals for the G&W power line sensor (blue bars) and PT (red bars) had similar behavior. The greatest harmonic component of voltage signals was at 60 Hz for phase A, B, and C (Figure 24A, B, and C). The harmonic components of voltage signals at 0 Hz were greater than for the BC (non-grounding) electrical fault test event (Figure 22A, B, and C), because the test event corresponds to a grounding electrical fault (ABCG). In Figure 24B and C, the G&W power line sensor (blue bars) and PT (red bars) harmonic components of voltage signals matched at high frequencies because of the ringing voltage behavior in Figure 24E and F.

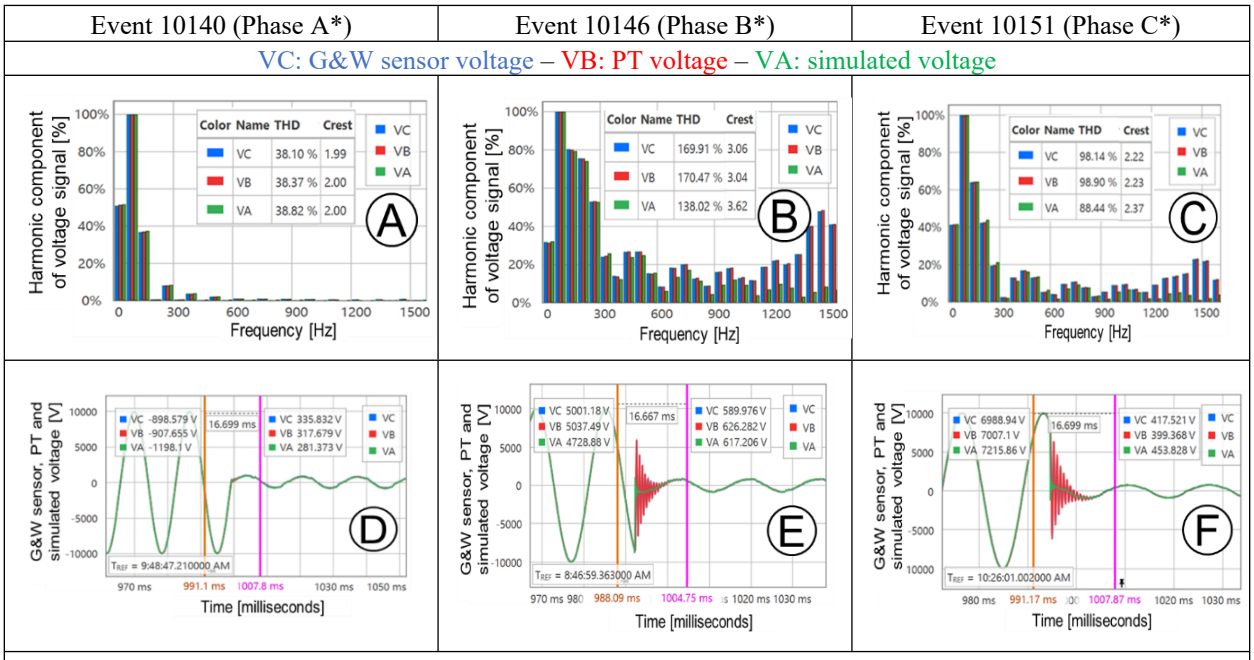

Figure 24. Phase A, B, and C voltage harmonic components (A, B, C) and voltage signals (D, E, F) for the G&W power line sensor, PT/CT, and simulated power grid at the load 26 feeder and ABCG electrical fault in power line section 34.

The measured harmonic components of current signals (Figure 25A, B, and C) and current signals (Figure 25D, E, and F) for the G&W power line sensor, PT/CT, and simulated power grid at the load 26 feeder and the BC electrical fault in power line section 34 are shown from Events 10140 (phase A), 10146 (phase B), and 10151 (phase C). The measured harmonic components of current signals for phase A (Figure 25A), B (Figure 25B), and C (Figure 25C) were plotted for a one-cycle transient event (approx. 16.6 ms). In Figure 25A, B, and C, the harmonic components of current signals for the G&W power line sensor (blue bars) and PT (red bars) had similar behavior. The greatest harmonic component of voltage signals was at 60 Hz for phase A, B, and C (Figure 25A, B, and C). The harmonic components of current signals at 0 Hz were greater than for the BC (non-grounding) electrical fault test event (Figure 23A, B, and C) because the test event corresponds to a grounding electrical fault (ABCG). In Figure 25A, B, and C, the G&W power line sensor (blue bars) and CT (red bars) harmonic components of current signals matched with a slight difference because of the minor noise of the current signals (Figure 25D, E, and F).

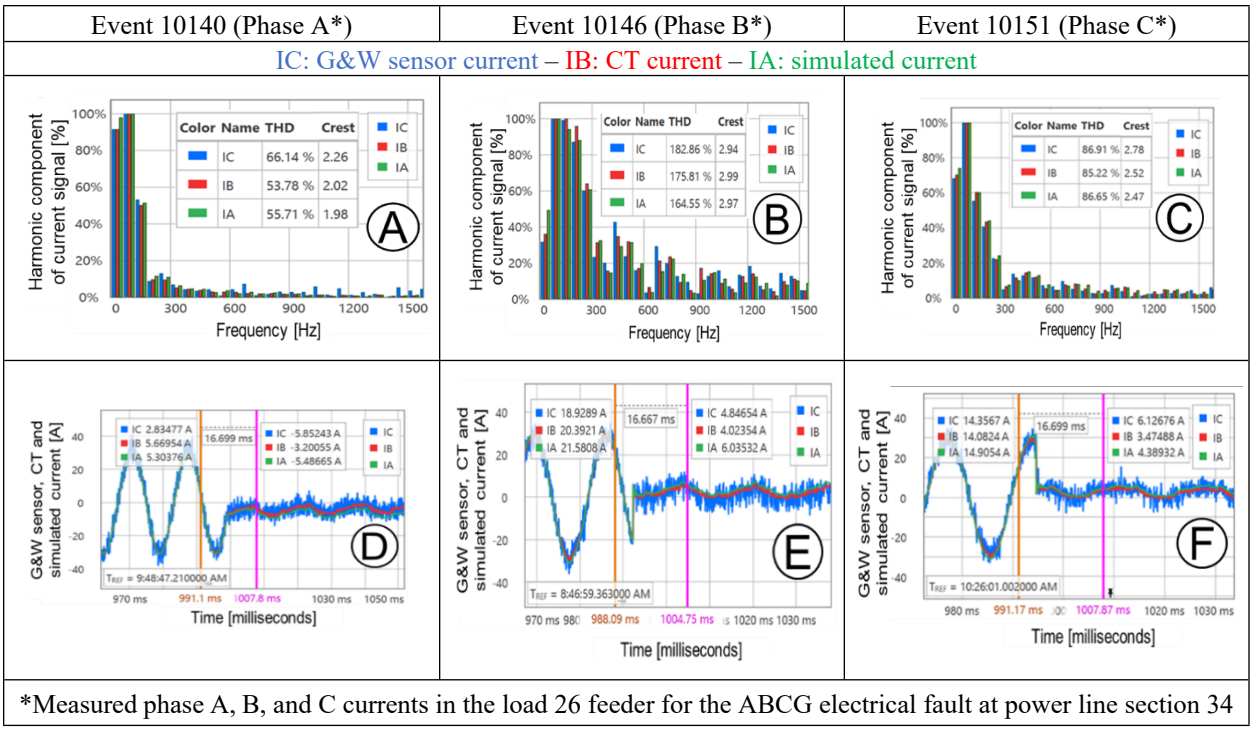

*Measured phase A, B, and C currents in the load 26 feeder for the ABCG electrical fault at power line section 34

Figure 25. Phase A, B, and C current harmonic components (A, B, C) and current signals (D, E, F) for the G&W power line sensor, PT/CT, and simulated power grid at the load 26 feeder and ABCG electrical fault in power line section 34.

6.6 ADVANCED OPLST WITH THE OP4510 REAL-TIME SIMULATOR AND SEL-735 POWER METER

In the OPLST with the OP4510 real-time simulator and SEL-735 power meter, the current and voltage signals from the G&W power line sensor, PT/CT, and simulated power grid were collected by the SEL-735 power meter. There, the voltage and current signals of phase A, B, and C correspond to the simulated power grid, PT/CT, and G&W power line sensor, respectively. In this way, the measured voltage and current signals from the simulated power grid, PT/CT, and G&W power line sensor were compared on the same referenced platform.

Electrical utilities have used PTs and CTs for several decades, and PTs and CTs have been tested with procedures based on the IEEE C57-13 2016 Std. [6]. However, new OPLSs based on advanced technologies (voltage divider, Rogowski coil, and optical principles) do not have testing procedures based on electrical apparatus or instrument standards. Therefore, assessment of these advanced OPLS is crucial. In this work, the comparison test procedure for the G&W power line sensor vs. the PT/CT was an effective method to evaluate the performance of these advanced technologies vs. iron core measurement transformers.

7. CONCLUSIONS AND FUTURE WORK

In this study, a 20/34.5 kV OPLST was installed for testing a G&W power line sensor with a traditional iron core PT/CT. The 20/34.5 kV OPLST with an OP4510 real-time simulator and SEL-735 power meter was run satisfactorily at different power grid scenarios, such as electrical fault, capacitor bank operation, and load feeder switch scenarios.

The performance of the G&W power line sensor vs. the PT/CT was evaluated by comparing the behavior of the voltage and current signals and harmonic components at one-cycle transient test events. The total harmonic distortion and crest factors for the voltage and current signals for the G&W power line sensor, PT/CT, and simulated power grid were compared satisfactorily, and the total harmonic distortion and crest factor percentage errors were calculated, demonstrating a better performance of the G&W power line sensor for voltage signals than for current signals.

This novel 20/34.5 kV OPLST integrated an OP4510 real-time simulator with a SEL-735 power meter, which allowed not only for performing different power grid scenarios, but also for collecting the voltage and current signals of the G&W power line sensor, PT/CT, and simulated power grid at the same referenced platform. This method enabled assessing the G&W power line sensor vs. the PT/CT by a comparison test, analyzing the behavior of analog signals and harmonics.

In future work, advanced OPLSs will be compared for other power grid scenarios based on using distributed energy resources with inverter-based systems, and other OPLS technologies will be compared with traditional PTs/CTs. In addition, the 20/34.5 kV OPLST will enable testing of new power line sensors under different weather conditions, in the winter or summer, and with ultraviolet radiation effects.

8. REFERENCES

[1] O. S. E. Atwa, *Practical Power System and Protective Relays Commissioning*, Academic Press, Elsevier, 2019.

[2] E. C. Piesciorovsky and T. Karnowski, "Variable frequency response testbed to validate protective relays up to 20 kHz," *Electric Power Systems Research* 194, 2021,1–10.

[3] S. Das, "Sub-Nyquist rate ADC sampling in digital relays and PMUs: Advantages and challenges," *6th IEEE International Conference on Power Systems*, New Delhi, India, March 4–6, 2016, 1–6.

[4] A. Hargrave, M. J. Thompson, and B. Heilman, "Beyond the Knee Point: A Practical Guide to CT Saturation," *71st Annual Conference for Protective Relay Engineers*, College Station, Texas, March 26–28, 2018, 1–20.

[5] H. J. Altuve, N. Fischer, G. Benmouyal, and D. Finney, "Sizing Current Transformers for Line Protection Applications," *66th Annual Conference for Protective Relay Engineers*, College Station, Texas, April 8–11, 2013, 1–16.

[6] IEEE C57-13 2016, IEEE Standard Requirements for Instrument Transformers, IEEE Power and Energy Society.

[7] D. Timmons, J. M. Harris, and B. Roach, *The Economics of Renewable Energy*, Global Development and Environment (GDAE) Institute, Tufts University, Medford, Massachusetts, 2014.

[8] E. C. Piesciorovsky, T. Smith, and T. B. Ollis, "Protection schemes used in North American microgrids," *International Transactions on Electrical Energy Systems* 30, 2020, 1–28.

[9] S. Hong and M. Zuercher-Martinson, "Harmonics and Noise in Photovoltaic (PV) Inverter and the Mitigation Strategies," *Solectria Renewables* 1–7.

[10] W. C. Sze, "Comparators for Voltage Transformer Calibrations at NBS, Journal of Research of the National Bureau of Standards-C," *Engineering and Instrumentation* 69C(4), 1965, 257–263.

[11] T. M. Souders, "A Wide Range Current Comparator System for Calibrating Current Transformers," *IEEE Transactions on Power Apparatus and Systems* PAS-90(1), 1971, 318–324.

[12] *Substation Test Equipment Guidebook*, Vanguard Instruments, Revision I, December 26, 2018, 1–12.

[13] *Diagnostic testing of instrument transformers*, OMICRON, 2020.

[14] *EZCT-2KA Current Transformer Test Set*, Vanguard Instruments, Revision E, March 16, 2018, 1–6.

[15] G. Heuston, "Doble® Testing Voltage (Potential) Transformers and Metering Units," *74th Annual International Doble Client Conference*, Boston, Massachusetts, April 26, 2007, 1–90.

[16] D. M. Parker and N. D. McCollough, "Medium-Voltage Sensors for the Smart Grid: Lessons Learned," *2011 IEEE Power and Energy Society General Meeting*, Detroit, Michigan, July 24–28, 2011, 1–7.

[17] F. Rahmatian, "High-Voltage Current and Voltage Sensors for a Smarter Transmission Grid and their Use in Live-Line Testing and Calibration," *2011 IEEE Power and Energy Society General Meeting*, Detroit, Michigan, July 24–28, 2011, 1–3.

[18] E. C. Piesciorovsky and M. E. Morales Rodriguez, "Assessment of the Phase to Ground Fault Apparent Admittance Method with Phase/Ground Boundaries to Detect Types of Electrical Faults for Protective Relays Using Signature Library and Simulated Events," *International Transactions on Electrical Energy Systems* 2022, 1951836.

[19] 7228 Operator's Manual, Single-Channel Industrial Amplifier for Demanding, High-Power Systems, AE TECHRON, 97-8004188_08-31-2020. Available online (accessed September 1, 2022): https://aetechron.com/pdf/7228_OperatorManual.pdf.

[20] Differential Probe for Power Management- Model 4232, Technical Data Sheet, Probe Master. Available online (accessed September 1, 2022): https://probemaster.com/4232-differential-probe-1-10-100-25-mhz-1400v/.

[21] Ultrastab 866 Precision Current Transducer, User Manual, Manufacturer: Danfysik A/S, Distributor: GMW Associates. February 12, 2002. Available online (accessed September 1, 2022): https://pdf4pro.com/amp/view/ultrastab-866-precision-current-transducer-user-manual-423ee8.html.

[22] SEL-735 Power Quality and Revenue Meter Instruction Manual, Schweitzer Engineering Laboratories Inc. Available online (accessed September 1, 2022): https://selinc.com/products/735/docs/.

[23] R. Tan, AC Time Overcurrent Relay Block MATLAB model, Version 1.0, June 2016. Available online (accessed September 1, 2022): https://www.mathworks.com/matlabcentral/fileexchange/57521-ac-time-overcurrent-relay-block.

[24] F. B. Costa, B. A. Souza, and N. S. D. Brito, "Effects of the fault inception angle in fault-induced transients," *IET Generation, Transmission & Distribution* 6, 2012, 463–471.

[25] M. Vadari, *Electric System Operations Evolving to the Modern Grid*, Artech House, Norwood, Massachusetts, 2013.

APPENDIX A. EVENTS OF MEASURED VOLTAGE AND CURRENT FOR PHASE A IN THE POWER GRID FEEDER

APPENDIX A. EVENTS OF MEASURED VOLTAGE AND CURRENT FOR PHASE A IN THE POWER GRID FEEDER

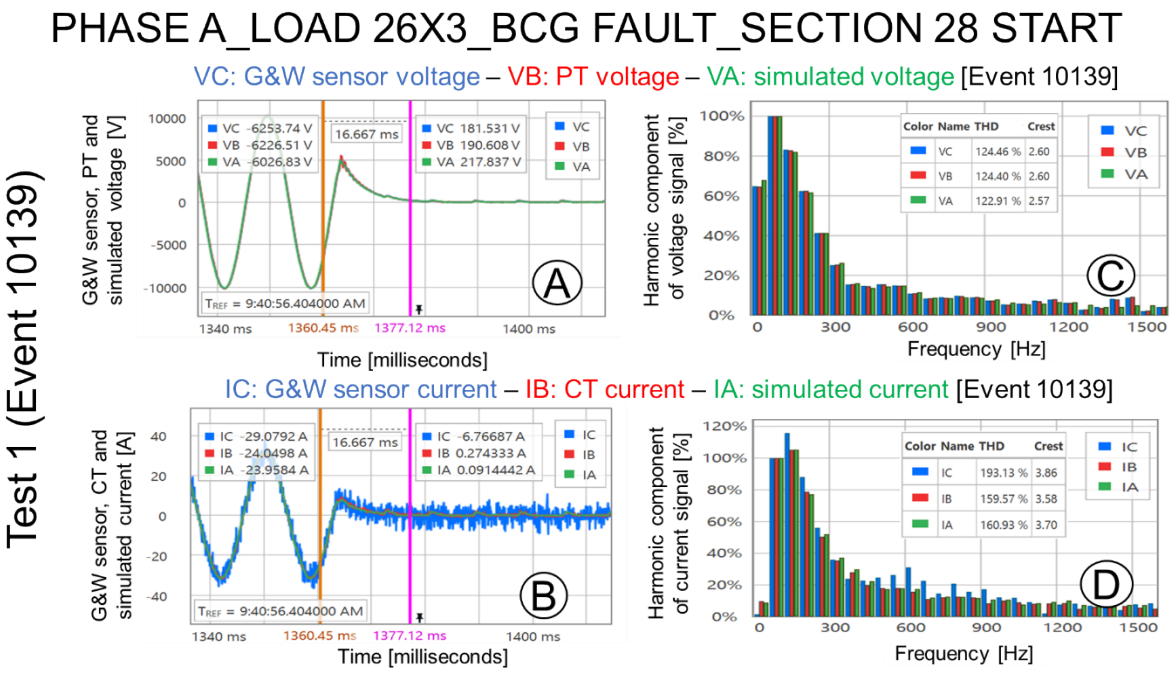

Figure A-1. Analog (A, B) and harmonic (C, D) plots of the G&W sensor, PT/CT, and simulated signals for phase A of the load 26 feeder at the BCG electrical fault in power line section 28.

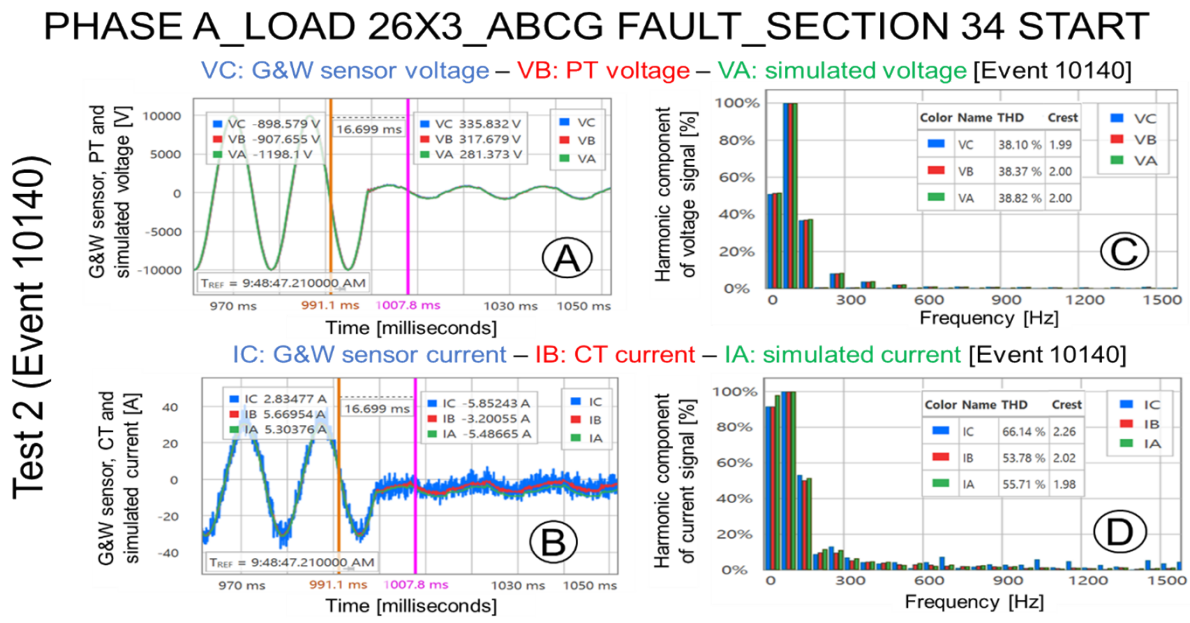

Figure A-2. Analog (A, B) and harmonic (C, D) plots of the G&W sensor, PT/CT, and simulated signals for phase A of the load 26 feeder at the ABCG electrical fault in power line section 34.

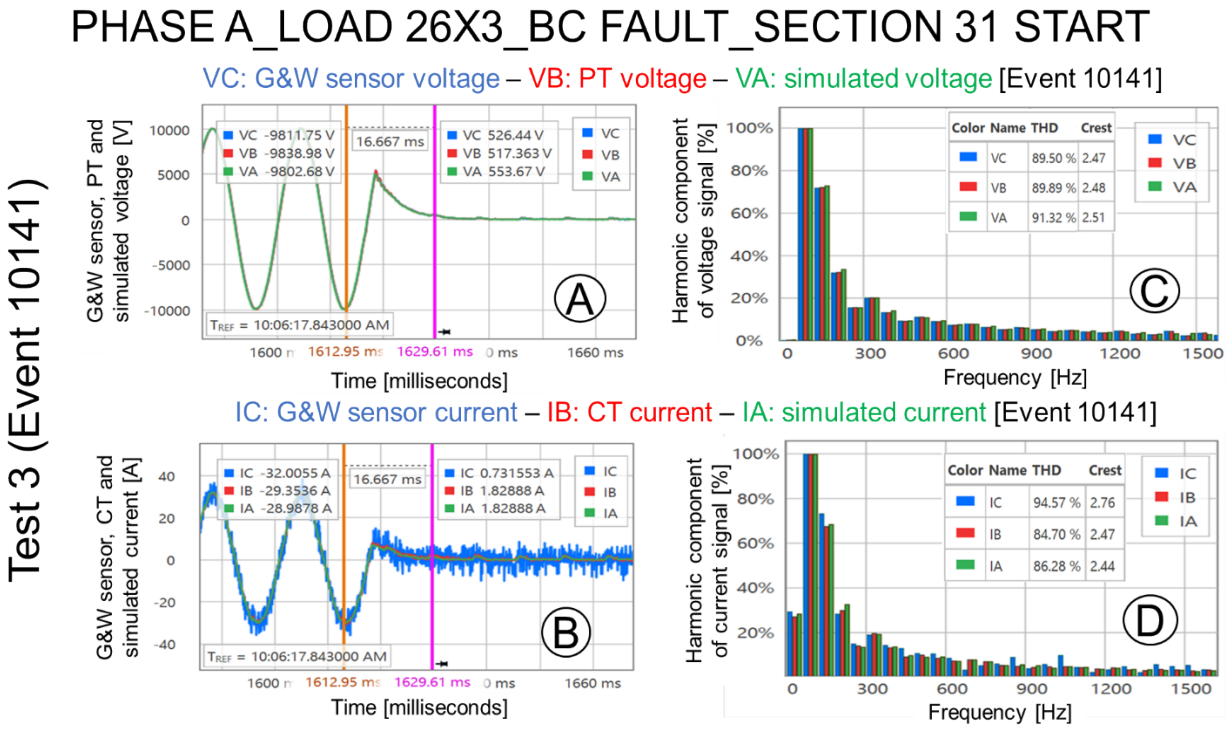

Figure A-3. Analog (A, B) and harmonic (C, D) plots of the G&W sensor, PT/CT, and simulated signals for phase A of the load 26 feeder at the BC electrical fault in power line section 31.

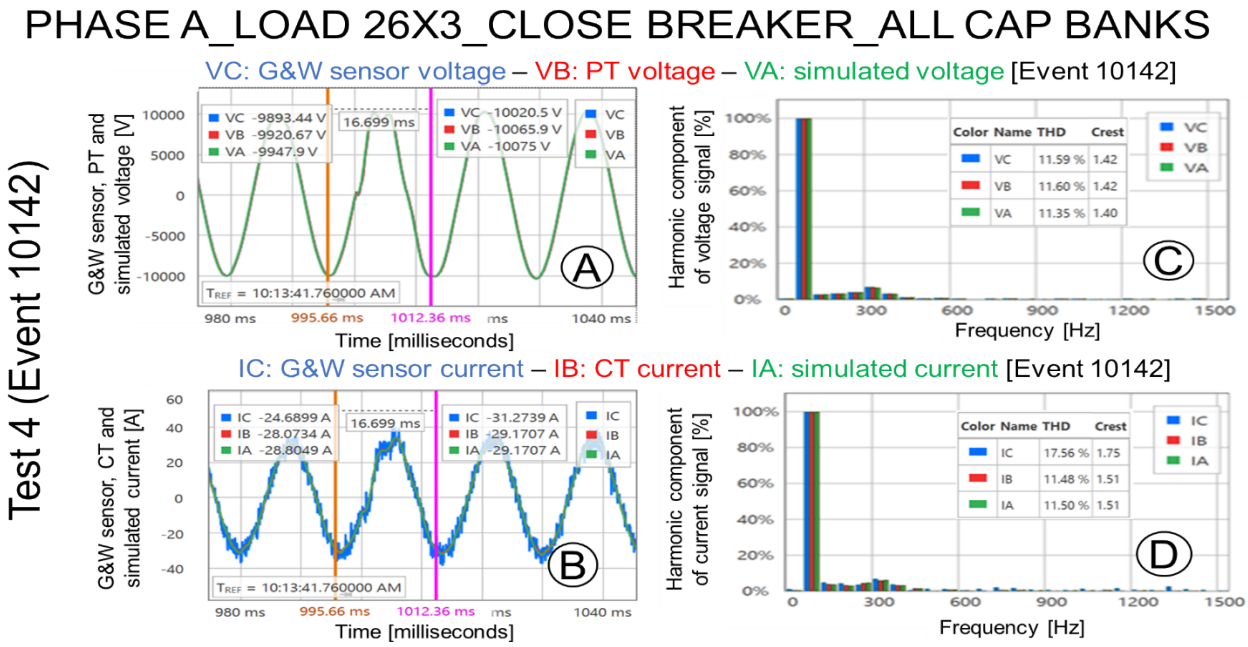

Figure A-4. Analog (A, B) and harmonic (C, D) plots of the G&W sensor, PT/CT, and simulated signals for phase A of the load 26 feeder when the capacitor banks are closed.

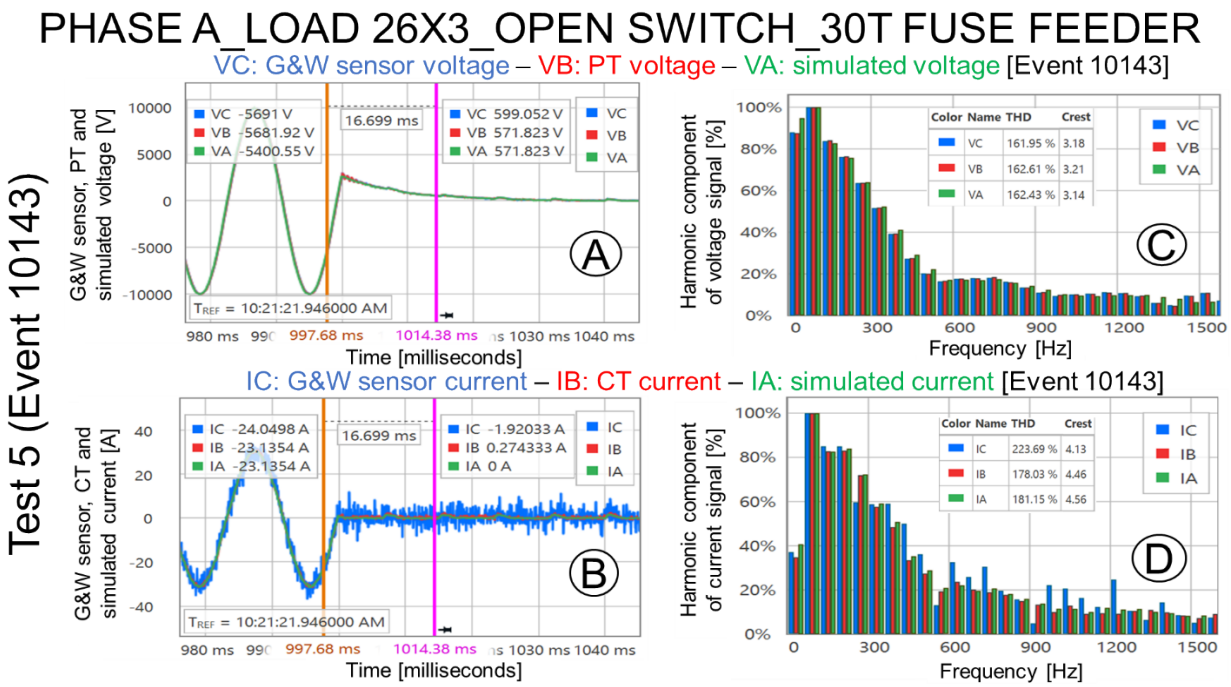

Figure A-5. Analog (A, B) and harmonic (C, D) plots of the G&W sensor, PT/CT, and simulated signals for phase A of the load 26 feeder at the opened switch.

APPENDIX B. EVENTS OF MEASURED VOLTAGE AND CURRENT FOR PHASE B IN THE POWER GRID FEEDER

APPENDIX B. EVENTS OF MEASURED VOLTAGE AND CURRENT FOR PHASE B IN THE POWER GRID FEEDER

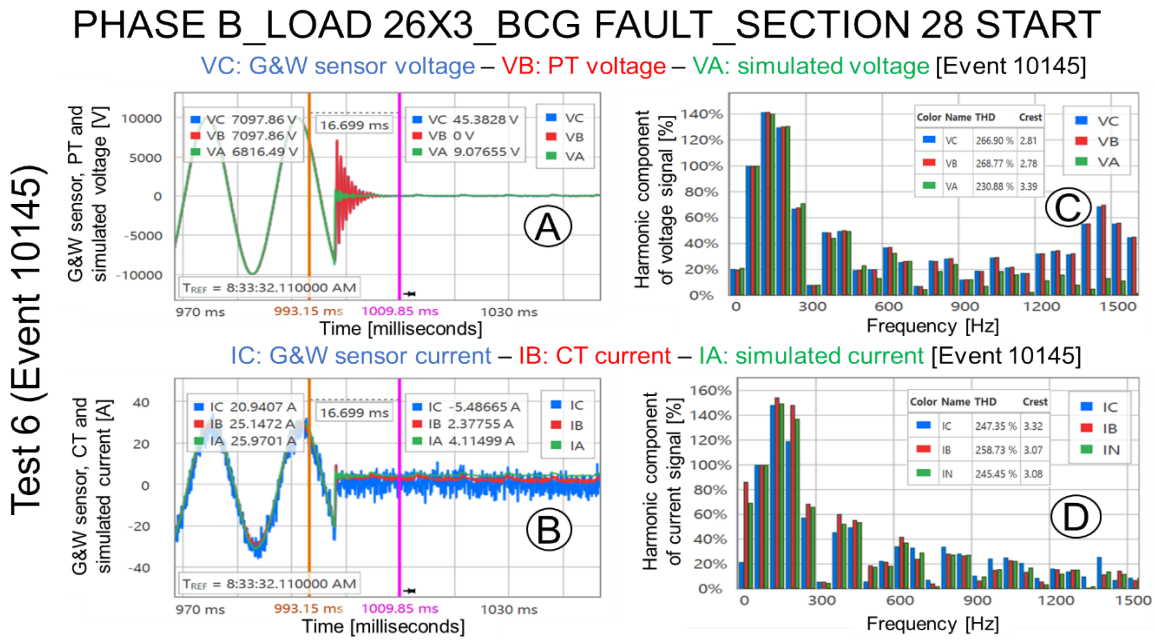

Figure B- 1. Analog (A, B) and harmonic (C, D) plots of the G&W sensor, PT/CT, and simulated signals for phase B of the load 26 feeder at the BCG electrical fault in power line section 28.

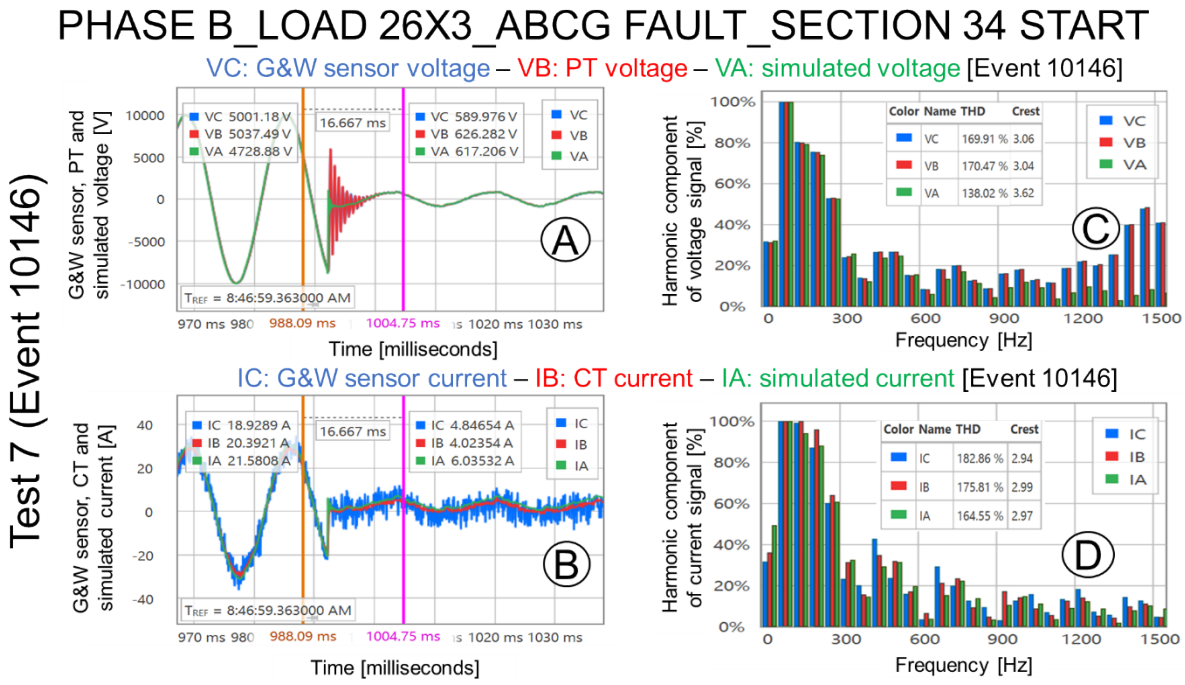

Figure B- 2. Analog (A, B) and harmonic (C, D) plots of the G&W sensor, PT/CT, and simulated signals for phase B of the load 26 feeder at the ABCG electrical fault in power line section 34.

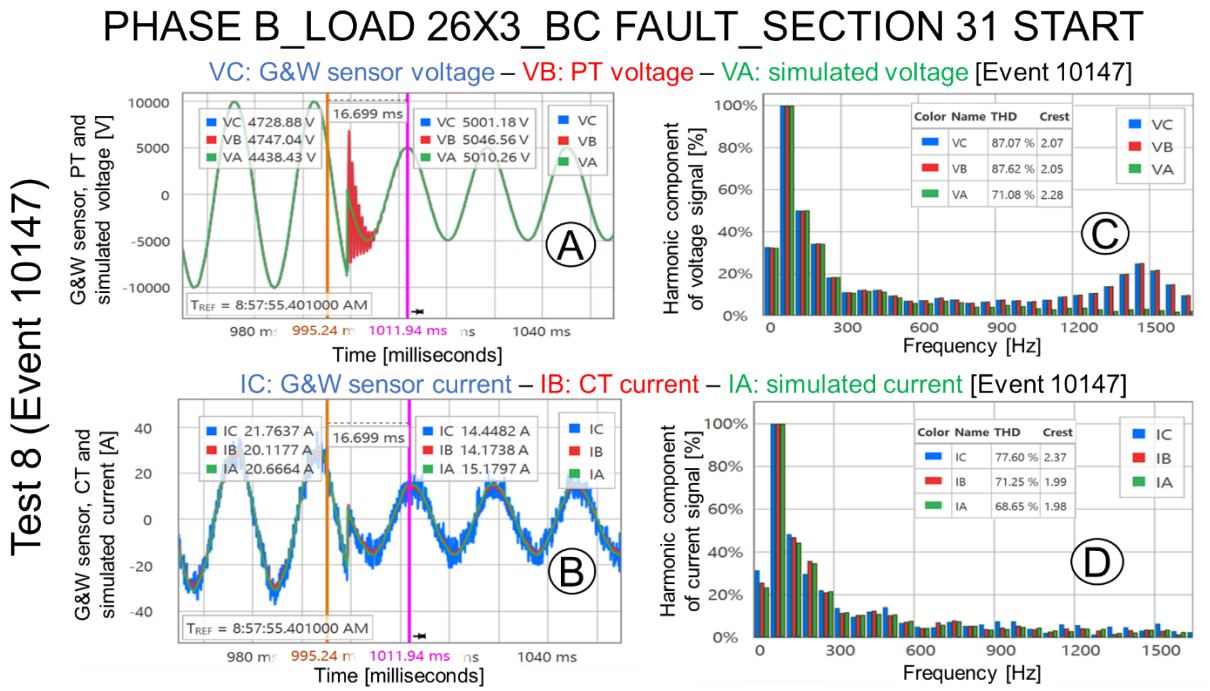

Figure B- 3. Analog (A, B) and harmonic (C, D) plots of the G&W sensor, PT/CT, and simulated signals for phase B of the load 26 feeder at the BC electrical fault in power line section 31.

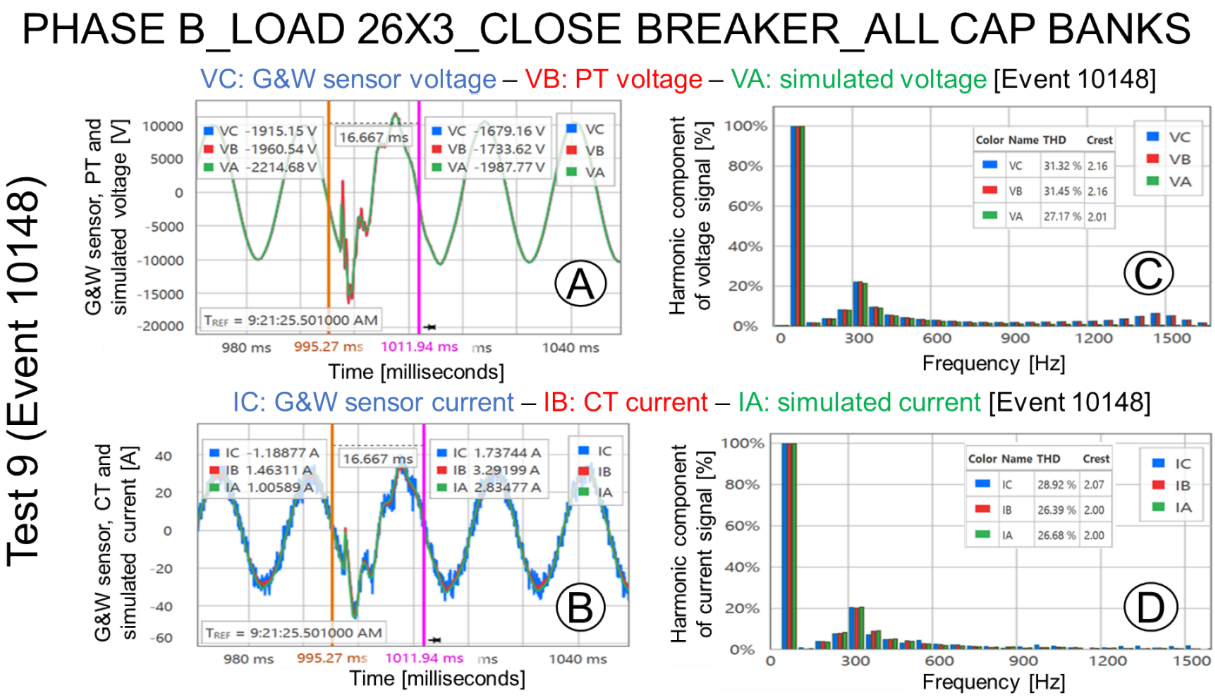

Figure B- 4. Analog (A, B) and harmonic (C, D) plots of the G&W sensor, PT/CT, and simulated signals for phase B of the load 26 feeder when the capacitor banks are closed.

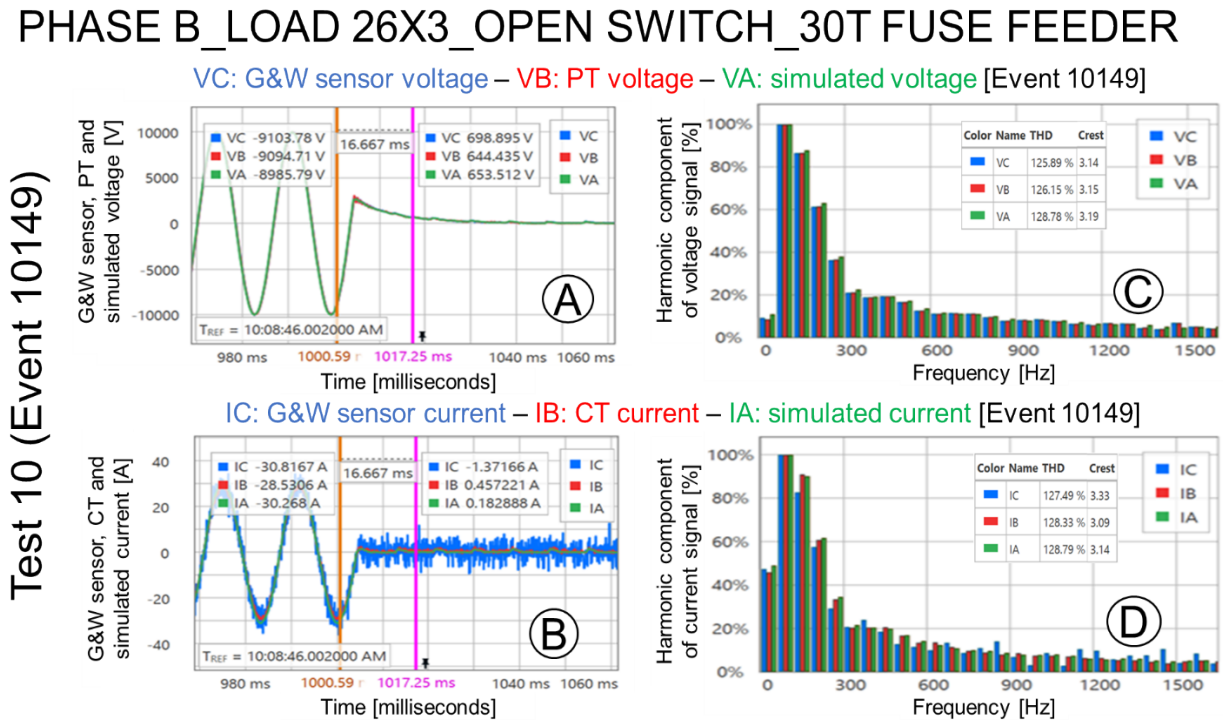

Figure B- 5. Analog (A, B) and harmonic (C, D) plots of the G&W sensor, PT/CT, and simulated signals for phase B of the load 26 feeder at the opened switch.

APPENDIX C. EVENTS OF MEASURED VOLTAGE AND CURRENT FOR PHASE C IN THE POWER GRID FEEDER

APPENDIX C. EVENTS OF MEASURED VOLTAGE AND CURRENT FOR PHASE C IN THE POWER GRID FEEDER

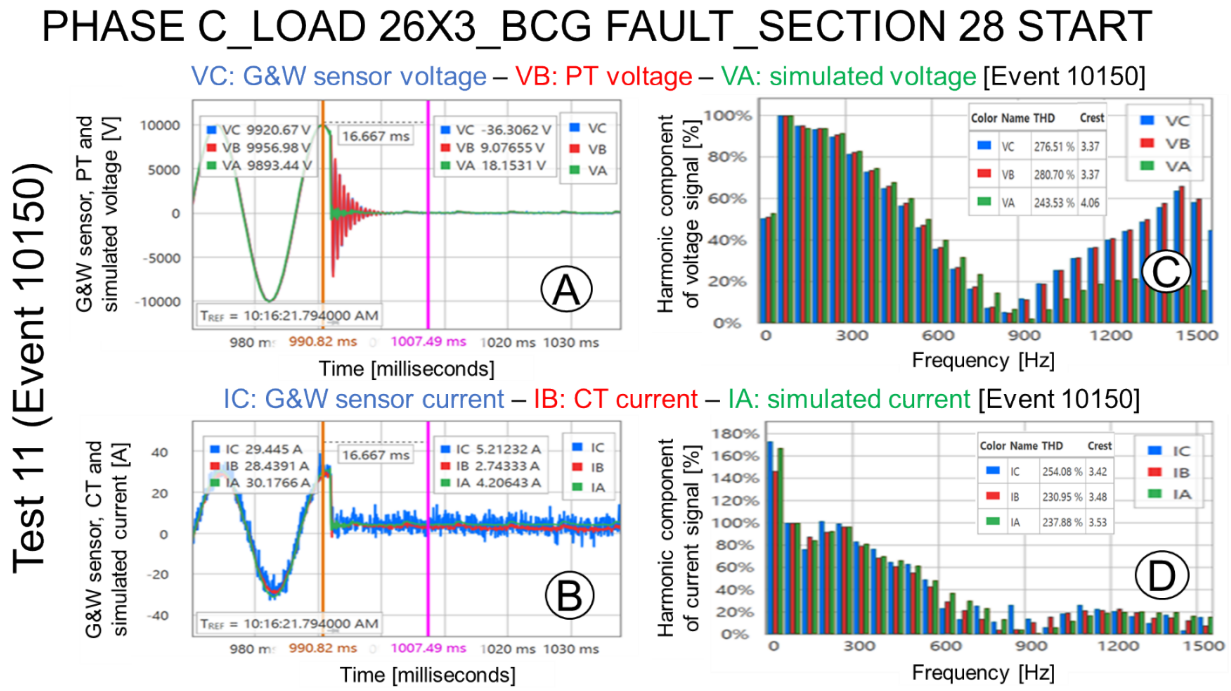

Figure C- 1. Analog (A, B) and harmonic (C, D) plots of the G&W sensor, PT/CT, and simulated signals for phase C of the load 26 feeder at the BCG electrical fault in power line section 28.

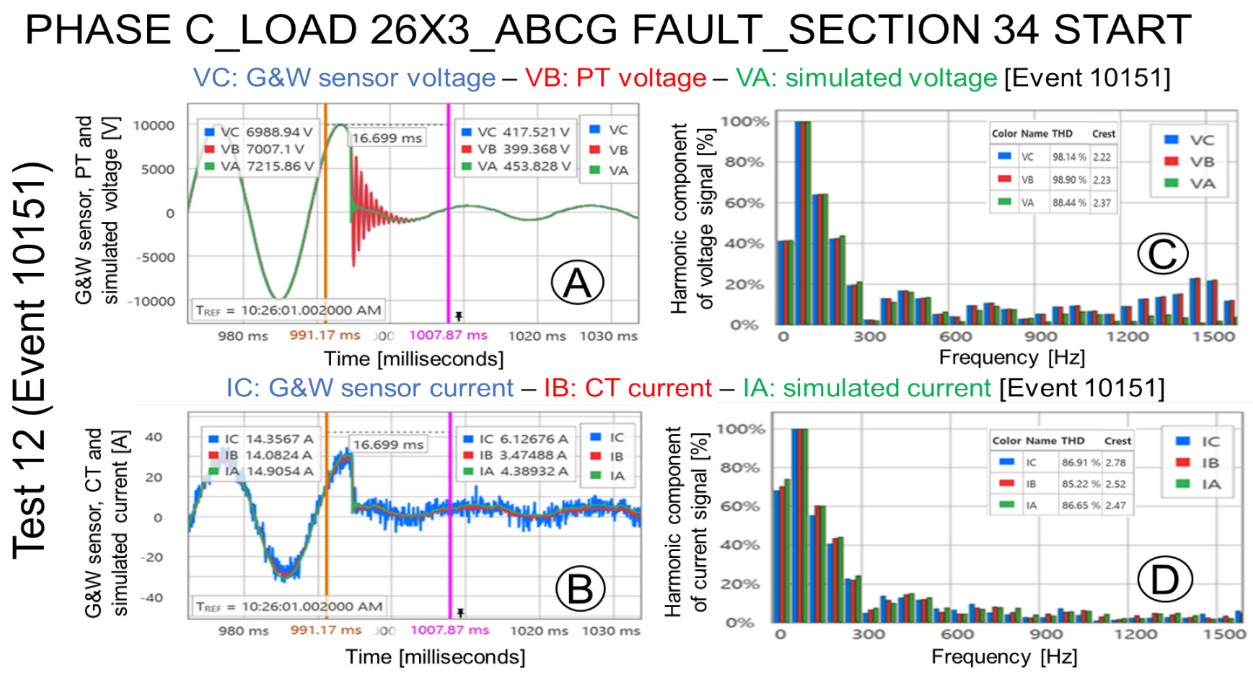

Figure C- 2. Analog (A, B) and harmonic (C, D) plots of the G&W sensor, PT/CT, and simulated signals for phase C of the load 26 feeder at the ABCG electrical fault in power line section 34.

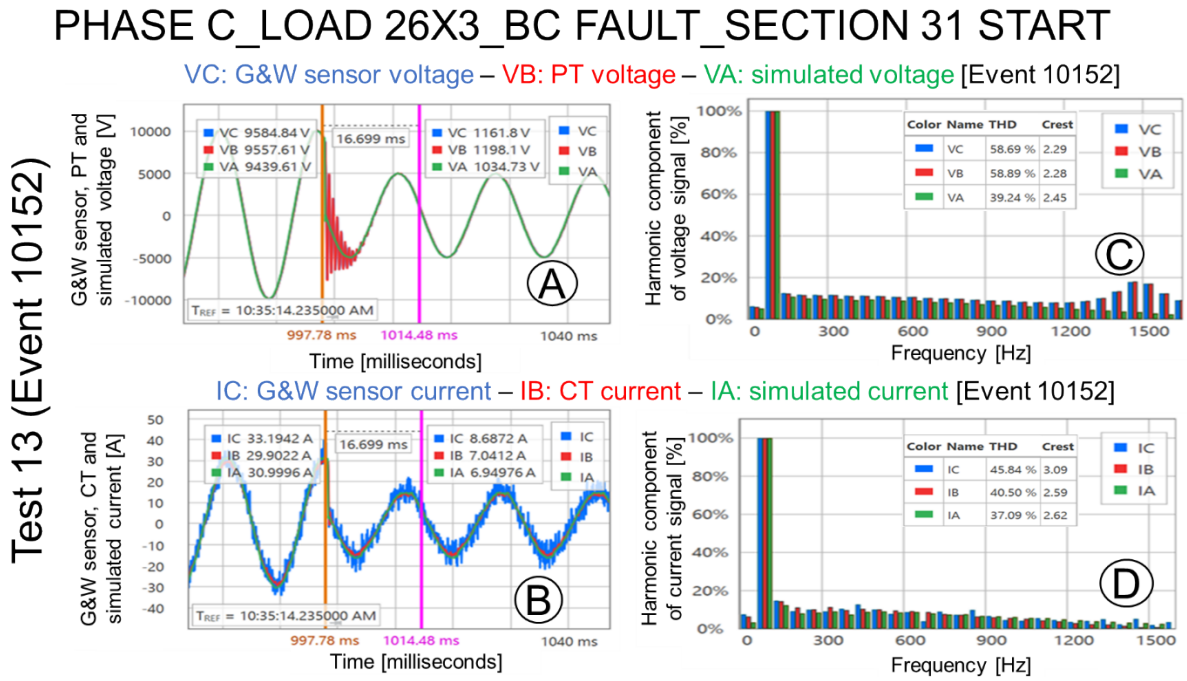

Figure C- 3. Analog (A, B) and harmonic (C, D) plots of the G&W sensor, PT/CT, and simulated signals for phase C of the load 26 feeder at the BC electrical fault in power line section 31.

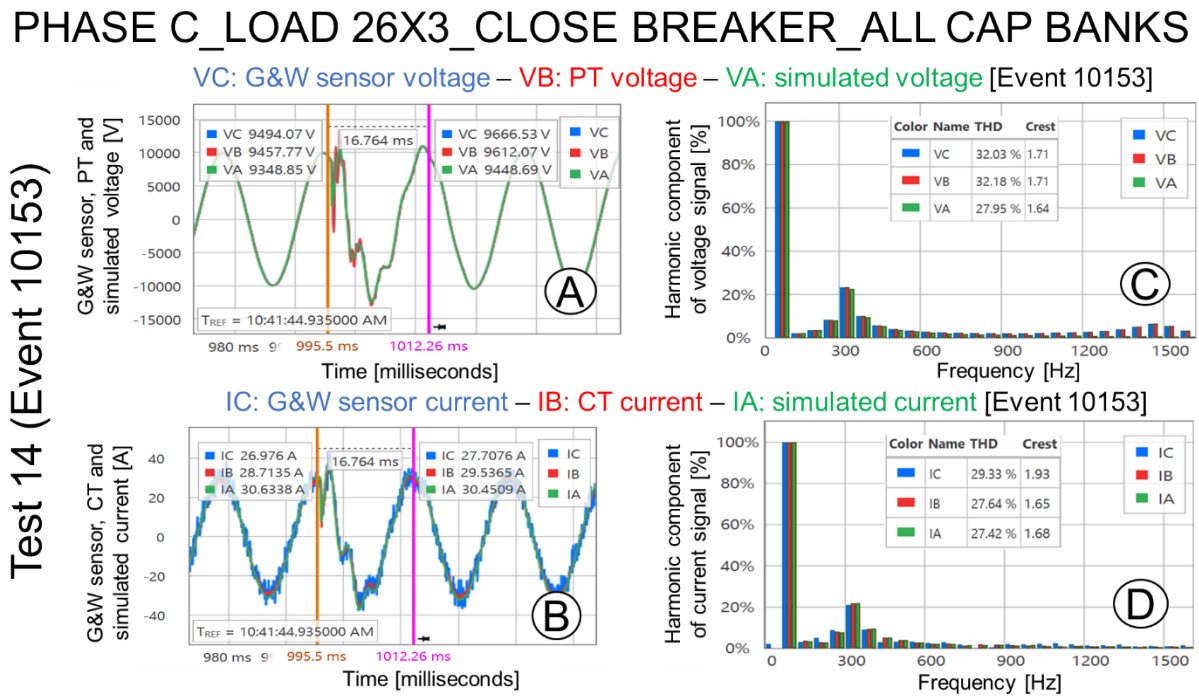

Figure C- 4. Analog (A, B) and harmonic (C, D) plots of the G&W sensor, PT/CT, and simulated signals for phase C of the load 26 feeder when the capacitor banks are closed.

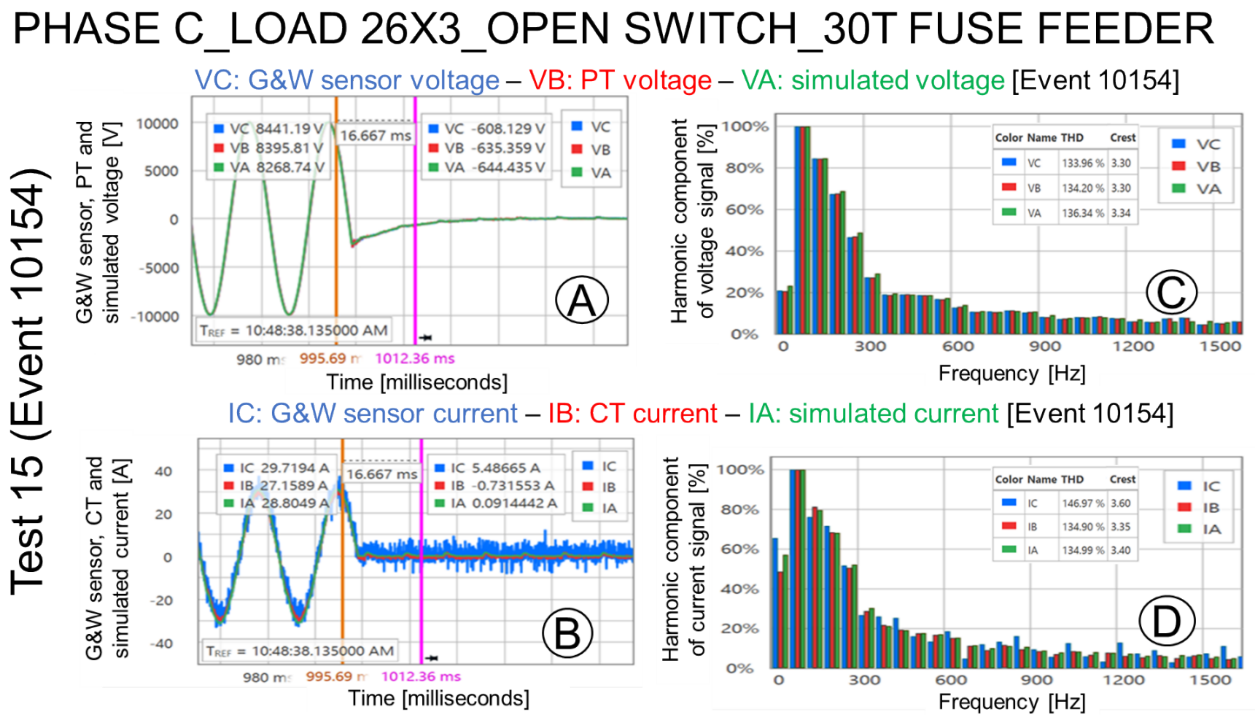

Figure C- 5. Analog (A, B) and harmonic (C, D) plots of the G&W sensor, PT/CT, and simulated signals for phase C of the load 26 feeder at the opened switch.